END
DATE
FILMED
2-81
DTIC

MICROCOPY RESOLUTION TEST CHART

NATIONAL BUREAU OF STANDARDS-1963-A

LEVEL

A076237

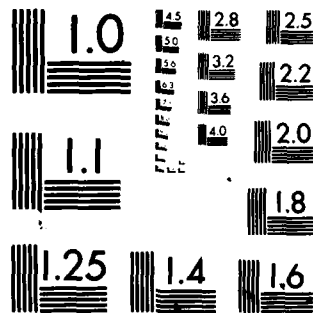# HIGH-ENERGY ION IMPLANTATION FOR MULTIGIGABIT-RATE GaAs INTEGRATED CIRCUITS

AD A093103

RCA Laboratories
Princeton, New Jersey 08540

DTIC
ELECTE
DEC 1 9 1980
C

OCTOBER 1980

ANNUAL REPORT
for the period 15 May 1979 to 30 June 1980

Approved for public release; distribution unlimited.
Reproduction in whole or in part is permitted for
any purpose of the US Government.

Prepared for
Office of Naval Research
Arlington, Virginia 22217
Contract No. N00014-78-C-0367
Contract Authority: NR 383-046

DDC FILE COPY

80 12 19 095

REPORT DOCUMENTATION PAGE		READ INSTRUCTIONS BEFORE COMPLETING FORM
1. REPORT NUMBER	2. GOVT ACCESSION NO. AD-A09? 103	3. RECIPIENT'S CATALOG NUMBER
4. TITLE (and Subtitle) HIGH-ENERGY ION IMPLANTATION FOR MULTIGIGABIT-RATE GaAs INTEGRATED CIRCUIT		5. TYPE OF REPORT & PERIOD COVERED Annual Report 15 May 79 - 28 Jun 80 (5-15-79 to 6-30-80)
		6. PERFORMING ORG. REPORT NUMBER PRRL-80-CR-37
7. AUTHOR(s) S. G./Liu, C. P./Wu, C. W./Magee		8. CONTRACT OR GRANT NUMBER(s) N00014-78-C-0367
9. PERFORMING ORGANIZATION NAME AND ADDRESS RCA Laboratories Princeton, New Jersey 08540		10. PROGRAM ELEMENT, PROJECT, TASK AREA & WORK UNIT NUMBERS PE 62762N RF 54-582-001 NR 383-046
11. CONTROLLING OFFICE NAME AND ADDRESS Office of Naval Research Arlington, Virginia 22217		12. REPORT DATE October 80
		13. NUMBER OF PAGES 64
14. MONITORING AGENCY NAME & ADDRESS (if different from Controlling Office) FS4582 RF545200 1		15. SECURITY CLASS. (of this report) Unclassified
		15a. DECLASSIFICATION/DOWNGRADING SCHEDULE N/A
16. DISTRIBUTION STATEMENT (of this Report) Approved for public release; distribution unlimited.		
17. DISTRIBUTION STATEMENT (of the abstract entered in Block 20, if different from Report)		
18. SUPPLEMENTARY NOTES		
19. KEY WORDS (Continue on reverse side if necessary and identify by block number) High-energy ion implantation Multigigabit-rate GaAs ICs Semi-insulating GaAs Laser annealing		

20. ABSTRACT (Continue on reverse side if necessary and identify by block number)

This Annual Report describes results of continued investigation on the implantation and activation of donors in semi-insulating (SI) GaAs, under Contract No. N00014-78-C-0367. These investigations include implantation of ^{28}Si up to an energy of 1.2 MeV and annealing of implanted layers by using laser irradiation and by using an electron beam.

DD FORM 1473
1 JAN 73

20.

Significant progress was made during this reporting period and the highlights are summarized below:

1. Uniformly doped, 1-μm-thick n-layers with (N_D - N_A) of 2×10^{17} cm^{-3} and $\mu(300)$ of 4450 cm^2/V-s were produced by multiple ^{28}Si implantation and capless thermal annealing under arsenic overpressure.

2. Temperature dependence of electrical activation by capless annealing under arsenic overpressure was studied over a range of 825-1000°C. For high-dose ($>10^{13}$ cm^{-2}) implants, the electrical activation increased with increasing temperature. No significant difference was found in the activation of low-dose ($<10^{13}$ cm^{-2}) ^{28}Si implants.

3. The redistribution of Cr from Cr-doped SI GaAs substrates due to implantation of ^{28}Si and subsequent annealing was studied by secondary ion mass spectrometry (SIMS). The Cr redistribution in thermally annealed ^{28}Si implants shows a strong dependence on implant dose. No significant redistribution was found for doses typically used for FET fabrication (2×10^{12} cm^{-2}). At higher dose levels, pulsed-laser-irradiated samples showed lower Cr redistribution than thermally annealed samples.

4. Preliminary studies on ^{40}Ar implanted samples showed Cr-redistribution effects similar to that of ^{28}Si implanted GaAs suggesting that the redistribution is due to implant damage.

5. The Cr redistribution caused by Ar implantation (decrease in Cr concentration) was exploited by ^{28}Si implantation into suitably Ar-bombarded samples. Activation of low-dose implants with high electron mobility was achieved.

6. Nonalloyed ohmic contacts were formed on laser-irradiated GaAs using Ti-Pt-Au metallization with good surface morphology. Double-frequency laser beam (λ = 1.06 and 0.53 μm) was used in the experiment.

7. The crystallinity of laser- (or electron beam) irradiated Si-implanted GaAs was studied using reflection high-energy electron diffraction (RHEED) analysis.

8. Preliminary studies on co-implant of ^{28}Si and ^{32}S into GaAs show higher mobility and activation when implants were annealed at a higher temperature.

9. Activation of 1-MeV implanted GaAs with peak electron density over 1×10^{19} cm^{-3} was demonstrated by using a high-power sub-bandgap Nd:Glass laser (λ = 1.06 μm).

10. The successful production of high-quality n-GaAs layers by direct implant of ^{28}Si into SI GaAs was demonstrated (in a concurrent program) by the fabrication of high-performance GaAs power FETs operating up to 26 GHz.

PREFACE

This annual report describes the research carried out at the Microwave Technology Center of RCA Laboratories during the period 15 May 1979 to 30 June 1980 in a program sponsored by the Office of Naval Research under Contract No. N00014-78-C-0367. F. Sterzer is the Center's Director and S. Y. Narayan is the Project Supervisor. The Project Scientist is S. G. Liu. Other Members of the Technical Staff working on the program are C. P. Wu and C. W. Magee. The Associate Staff contributing to this program are F. Kolondra, S. Jain, and F. C. Duigon. S. Manasian of Fusion Energy Corporation, Princeton, NJ, was responsible for the Van de Graaff generator used for high-energy implantation. J. T. McGinn and J. H. Thomas of RCA Laboratories carried out the RHEED and Auger analyses, respectively.

Accession For		
NTIS GRA&I	☑	
DTIC TAB	☐	
U·announced	☐	
Justification		
By		
Distribution/		
Availability Codes		
Dist	Avail and/or Special	
A		

TABLE OF CONTENTS

LIST OF ILLUSTRATIONS

LIST OF ILLUSTRATIONS (Continued)

LIST OF TABLES

SECTION I

INTRODUCTION

This report describes our work during the past twelve months on the ONR-sponsored program started in May 1978. The objectives of the program are: (1) study of high-energy ion implantation of donors into GaAs for multigigabit-rate GaAs integrated-circuit development, and (2) annealing of implanted GaAs using high-power lasers to remove lattice damage and activate implanted donors.

The work performed prior to this reporting period was described in a previous Annual Report (August 1979, Contract No. N00014-78-C-0367). The highlights of that report are summarized to provide a baseline for discussion.

- We have investigated implantation of $^{28}Si^+$ into semi-insulating (SI) GaAs with implant energies ranging from 40 keV to 1.2 MeV. The profiles and range statistics of ^{28}Si-implanted GaAs were studied using secondary ion mass spectrometry (SIMS), and based on the information obtained, uniformly doped $\sim$1-μm-deep ^{28}Si profiles were produced in GaAs using multiple implants.

- We have developed a capless thermal annealing process under arsenic overpressure which results in high activation efficiency with excellent surface morphology. The arsenic overpressure was produced by introducing AsH_3 and H_2 into the annealing furnace.

- We have investigated laser-annealing of Si-implanted GaAs using a high-power Nd:Glass laser and a ruby laser. Electrical activation of high-dose, low-energy (<300 keV) implanted samples is many times higher in laser-annealed samples than for those thermally annealed. No activation was obtained in laser-irradiated samples with implant doses of less than upper $\sim$10^{13} cm^{-2}.

- We have demonstrated nonalloyed ohmic contacts formed by direct evaporation of AuGe onto high-dose implanted laser-irradiated GaAs surface.

- We have studied impurity distribution in as-implanted, thermally annealed, and laser-annealed samples by SIMS. The amount of impurity redistribution depends on the energy and the dose of implantation and on the energy density of the annealing laser pulse. Substantial impurity broadening was observed in the high-dose implanted samples irradiated with a high-energy density ($\sim$2 J/cm^2) pulse. Anomalous

1

"shoulder broadening" effect was also observed in the SIMS profile of thermally annealed, high-dose Si-implanted samples.

- We have studied optical absorption in Si-implanted GaAs wafers irradiated with high-power laser pulse. Measurements show that implantation-enhanced absorption at a given infrared wavelength increases with implant dose. This enhanced absorption is greatly reduced following laser irradiation due to lattice reordering.

- We have studied electrical activation as a function of fluences in Si-implanted GaAs capless annealed at a given temperature. The carrier concentrations are limited at the high dose to about 3×10^{18} cm^{-3}, and at the low dose to about 5×10^{16} cm^{-3} following annealing at 825°C for 20 minutes. A threshold dose was observed below which the implanted layer was no longer activated, or activated with poor mobility. This cutoff dose depends on the substrate characteristics and is typically $\sim 2 \times 10^{12}$ cm^{-2} for 200-keV implantation.

- We have studied implantation of $^{32}S^{+}$ in GaAs and its characteristics following capless annealing. The measured depth distribution of electron concentration is broader for S-implanted than for Si-implanted GaAs as a result of thermal diffusion during annealing. The diffusion coefficient at 825°C for S and Si in GaAs was deduced from the electron density profiles (for low dose $\leq 10^{13}$ cm^{-2} implant) to be $2-5 \times 10^{-14}$ and $\leq 10^{-15}$ cm^{2}/s, respectively.

During this reporting period we continued investigations in (1) Si-implantation and capless annealing; (2) laser and electron beam annealing; and (3) chromium redistribution in implanted and annealed GaAs. Significant progress made in these areas during this period includes:

(1) producing uniformly doped ~ 1-μm-deep n-layers at medium doping densities with good mobility;

(2) forming nonalloyed ohmic contacts on laser-irradiated GaAs with refractory metallization;

(3) improving low-dose threshold and mobility using an argon implant-gettering technique, which is the outcome of chromium redistribution studies in semi-insulating GaAs substrates.

2

Finally, in a concurrent program, high-performance GaAs power FETs operating up to 26 GHz were fabricated using Si-implanted and capless annealed n-layers on semi-insulating substrates.

SECTION II

Si IMPLANTATION AND CAPLESS ANNEALING

A. INTRODUCTION

Implantation of ^{28}Si into semi-insulating (SI) GaAs has been investigated
with implant energies ranging from 40 to 1200 keV [1-3], and fluences between
1×10^{12} and 5×10^{15} cm^{-2}. An operationally simple, capless annealing process
which results in high activation efficiency with good surface morphology has
been developed. In this section we will describe extended work and results on
Si-implant and thermal annealing performed during the past twelve months in
the current program.

B. MODIFICATION OF MeV-IMPLANTATION SYSTEM - VAN DE GRAAFF MACHINE

Implantations at energy levels above 500 keV were carried out using the
Van de Graaff machine that is capable of a mass-energy (atomic mass x energy
in MeV) product of ~33 with the available analyzing magnet. The implant area
was limited previously to 1 in. by 1 in. square, and some discrepancies had
been found between the implanted and the measured doses.

During this program period, a study of the ion beam intensity distribu-
tion showed a neutral region in the beam. The nonuniformity could account for
some discrepancies in the fluences observed previously. A test run made with
a small GaAs sample placed outside the neutral zone proved the system to
be otherwise operating properly. To solve the implant nonuniformity problem,
a 4° beam deflection system ("dog-leg") was constructed and installed to
eliminate the neutral particles in the beam. Furthermore, the target chamber

1. S. G. Liu, E. C. Douglas, and C. P. Wu, "High-Energy Ion Implantation for
    Multigigabit-Rate GaAs Integrated Circuit," Annual Report, May 15, 1978
    to May 14, 1979, under ONR Contract N00014-78-C-0367.
2. S. G. Liu, E. C. Douglas, C. P. Wu, C. W. Magee, S. Y. Narayan, S. T.
    Jolly, F. Kolondra, and S. Jain, "Ion Implantation of Sulfur and Silicon
    in GaAs," RCA Review 41, 227 (1980).
3. S. G. Liu, E. C. Douglas, C. W. Magee, F. Kolondra, and S. Jain, "High-
    Energy Implantation of Si in GaAs," Appl. Phys. Lett. 37, 79 (1980).

for the high-energy implant system was redesigned and constructed to increase the implant area from 7.56 cm^2 (square) to 13.07 cm^2 (circular, 4.08 cm in diameter). The ion beam intensity distribution was retested (by producing an image on paper) after the modifications, and it indeed showed a uniform distribution over a circular area of ∿4 cm in diameter. SIMS profiles of a 1-MeV Si-implanted GaAs wafer before and after thermal annealing are shown in Fig. 1. No Si redistribution was detected after capless annealing under arsenic pressure at 825°C for 20 min.
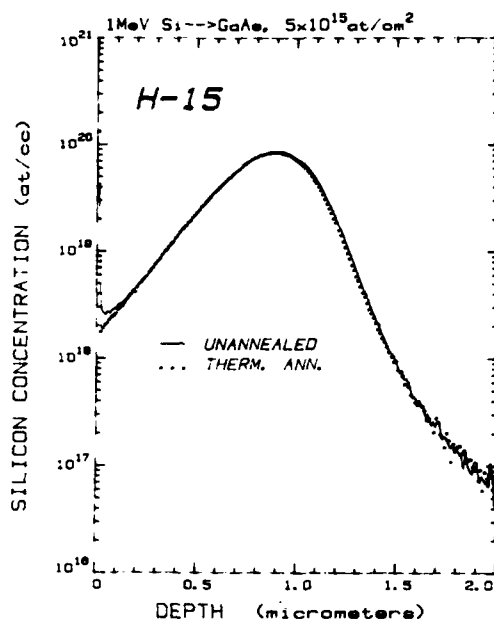
Figure 1. Impurity profiles of Si-implanted GaAs before and after thermal annealing at 825°C for 20 min.

Another modification was made to the high-energy implant system so that the system is capable of handling four different ion sources. Argon has been successfully implanted into GaAs at 750 keV in addition to implantation of ^{28}Si. Results of ^{40}Ar implantation are presented later in this section and in Section IV.

C. NEW THERMAL ANNEALING SYSTEM

Capless anneal of implanted GaAs is done under arsenic overpressure in an open quartz tube. The arsenic overpressure is maintained by using a flow of

5

AsH_3 and H_2. The temperature was limited to ~850°C in the system used previously. During this program period, a new annealing furnace was installed. The system allows much larger wafers (~1-1/2 in. diameter) to be annealed at a higher temperature (~1000°C) than previously and is a much cleaner system since it is used solely for annealing purposes. The wafer had a very clear surface after annealing and the activation was similar to wafers annealed in the older furnace.

D. MULTIPLE IMPLANTATIONS - DOPING PROFILE CONTROL

The profiles and range statistics of ^{28}Si implants in GaAs from 40 to 1200 keV have been analyzed using secondary ion-mass spectrometry (SIMS). The measured profiles are noticeably skewed and have been fitted using the first-four-moment Pearson technique [4,5]. Figure 2 shows reduction of the data to R_p and ΔR_p values corresponding to LSS Gaussian reduction techniques and first-four-moment Pearson techniques. Based on the information obtained, a ~1×10^{18} cm^{-3} doped, ~1-μm-deep electron density profile has been produced [1-3] in GaAs using multiple implants. Figure 3 shows the electron density profile measured by differential C-V technique in conjunction with layer removal controlled by chemical etching. An experimentally measured SIMS profile and its corresponding calculated profile were included for comparison. The wafer (H23) used for comparison had implant doses two orders of magnitude higher than the one used for electron density profile measurement.

During this program period, we further produced implanted n-layers with controlled electron density profiles to meet the requirement of device (MESFET) fabrication. Based on the range and straggle data deduced from the SIMS profiles made on Si-implanted GaAs samples, we designed multiple implantation profiles to produce (a) a flat 0.6- to 1.1-μm-thick n-layer at an electron density of ~$10^{17}/cm^2$ and (b) a high/low (n^+-n) profile which has an n^+-layer at the surface followed by the n-active layer. The n^+-layer is to facilitate good ohmic contacts. A computer program was used for the design. Table 1 shows the calculated implant conditions using four implants for achieving flat and n^+-n profiles, respectively, at an impurity concentration level of 1.5×10^{17} cm^{-3}.

4. M. G. Kendall and A. Stuart, The Advanced Theory of Statistics, (Charles Griffin, London, 1958), Vol. 1, p. 148.
5. W. P. Elderton, Frequency Curves and Correlation, (Cambridge University Press, 1953), 4th ed.
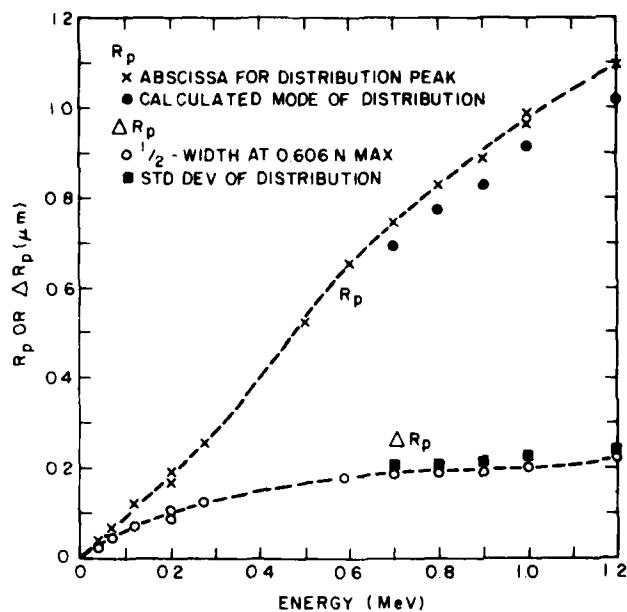
Figure 2. Reduction of data to R_p and ΔR_p values.
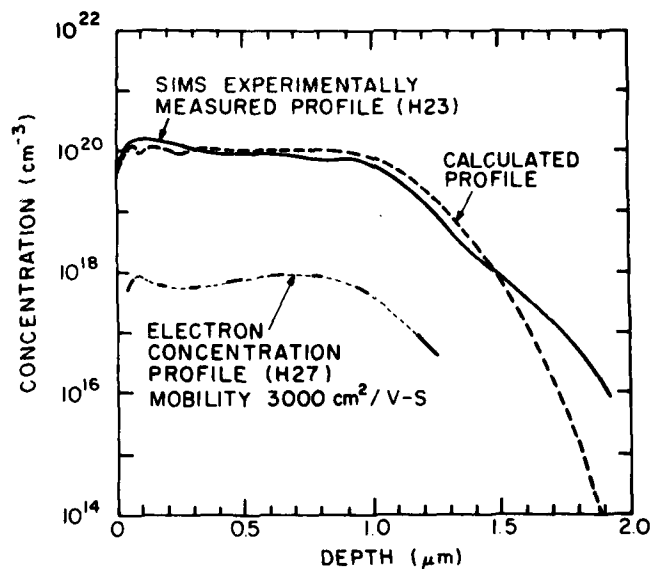
Figure 3. Comparison of calculated and actual SIMS profiles. Electron concentration profile of a sample with lower dose implants is also inclued.

7

TABLE 1.   CALCULATED MULTIPLE IMPLANT PARAMETERS FOR FLAT (H51,
           H52) AND HIGH-LOW (H53) PROFILES OF Si IN GaAs

H51 and H52		H53	
Energy (keV)	Dose (cm^{-2})	Energy (keV)	Dose (cm^{-2})
70	1.7×10^{12}	70	4.0×10^{13}
250	4.3×10^{12}	250	4.3×10^{12}
600	6.5×10^{12}	600	6.5×10^{12}
1000	7.0×10^{12}	1000	7.0×10^{12}

The corresponding implantation data are shown in Table 2. A comparison of
the calculated plot, the measured SIMS profile and carrier concentration
profile is given in Fig. 4 for the flat profile, and Fig. 5 for the n^{+}-n
profile.

TABLE 2.   IMPLANT CONDITIONS FOR FLAT (AT 1.5×10^{17} cm^{-3}) AND
           HIGH-LOW PROFILES OF Si IN GaAs

H51 and H52

Energy (keV)	70	250	600	1000
N_{dose} (cm^{-2})	1.7×10^{12}	4.3×10^{12}	6.5×10^{12}	7.0×10^{12}
Dose No.	32.1	27.4	19.3	20.9
Scale	2×10^{-7}	6×10^{-7}	6×10^{-7}	6×10^{-7}

H53

Energy (keV)	70	250	600	1000
N_{dose} (cm^{-2})	4.0×10^{13}	4.3×10^{12}	6.5×10^{12}	7.0×10^{12}
Dose No.	25.8	27.4	19.3	20.9
Scale	6×10^{-6}	6×10^{-7}	6×10^{-7}	6×10^{-7}

Area = 24.19 cm^2 Area = 11.40 cm^2

(Labs machine)   (FEC machine)

The agreement among the three profiles in Fig. 4 is reasonably good.
The abrupt decrease in carrier concentration at the tail end of the profile, as
compared to the calculated and the SIMS profiles, is believed related to the
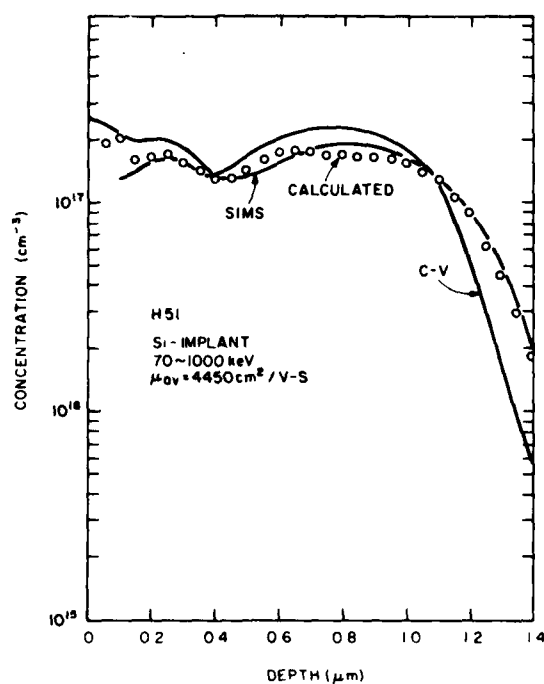
Figure 4. Multiple-implant profiles of H51: SIMS, carrier
concentration, and calculated.

low activation at low dose levels. The dip in the profile around 0.4 μm below
the surface is a result of approaching the limit of the two implant machines
used (one <300 keV, one >500 keV). These comments are also applicable to
Fig. 5; the greater discrepancy in Fig. 5 between the carrier concentration
profile and the calculated and SIMS profiles may be related to the higher
implant dose $(4x10^{13}$ cm$^{-2})$ for the n$^+$ implant. Higher implant dose results
in greater chromium redistribution in the SI substrate after thermal annealing;
therefore, it may cause anomalous behavior in electrical activation. Chromium
redistribution will be discussed in Section IV.

The carrier concentration and the Hall mobility profiles in multiple-
implanted thermally annealed GaAs samples were also measured using differential
van der Pauw measurement. Figure 6 shows the measured results on sample H51,
the ∿1-μm-deep implanted sample described above. The carrier concentration
profile agrees well with that determined from the differential C-V measurement
(Fig. 4). The mobility profile shows an average value between 4000 and 5000
cm^2/V-s.

Figure 7 shows the carrier concentration and mobility profiles of a 1-
MeV, 1x10^{13} cm^{-2} Si-implanted capless annealed GaAs sample (H37). The carrier
concentration profile is composed of both the van der Pauw and the differential
C-V measurements. It is interesting to note the high mobility (μ_{av} = 4520

9
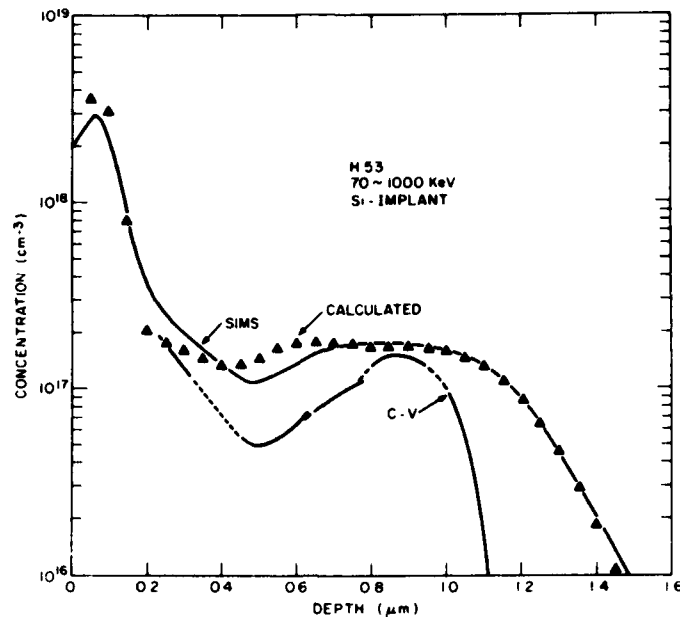
Figure 5. High-low dose multiple-implant profiles: SIMS, carrier concentration, and calculated.
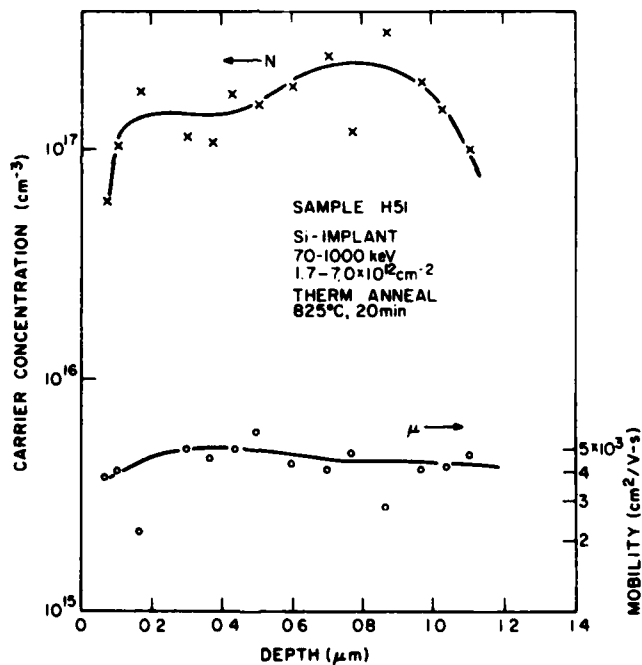
Figure 6. Carrier concentration and mobility profiles of sample H51.

cm^2/V-s) associated with this implanted sample. In particular, the mobility is maintained at a high level of $\sim$5000 cm^2/V-s as the doping density decreases to $\sim 10^{16}$ cm^{-3} toward the sample surface. This result was not observed in

10
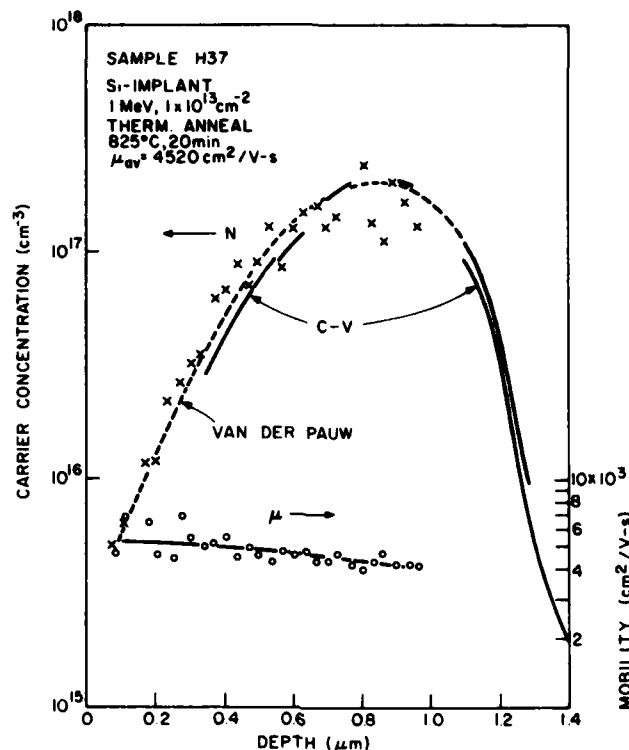
Figure 7. Carrier concentration and mobility profiles of sample H37.

low-dose ($<3 \times 10^{12}$ cm^{-2}), low-energy (~ 200 keV) implantation experiments. We speculate that this result may be related to the chromium redistribution in the SI GaAs substrate following implantation and annealing. As shown in Section IV, the chromium distribution depends on the amount of implant dose. In sample H37 (1 MeV, 1×10^{13} cm^{-2}), the chromium was depleted from 5×10^{16} cm^{-3} to $\sim 2-3 \times 10^{16}$ cm^{-3} in the surface layer following thermal annealing. The low chromium concentration could reduce compensation and allow low dose activation with higher mobility. Related experimental results will be described later in this section.

The electrical properties of high-energy implanted and capless annealed (825°C, 20 min) samples were evaluated using van der Pauw measurements [6]. The mobilities, carrier concentrations, and activation efficiencies of a

6. L. J. van der Pauw, "A Method of Measuring Specific Resistivity and Hall Effect of Discs of Arbitrary Shape," Philips Res. Rep. 13, 1 (1958).

number of wafers are shown in Table 3. The top five wafers (H51, H52, H53, H62 and H63) listed were multiple implanted, each receiving four implants to produce 1-μm-thick layers. The carrier concentration values listed were averaged over the 1-μm n-layer. Note the high mobilities and electrical activations obtained in the 1-μm layers with ~2x10^{17} cm^{-3} constant doping level.

TABLE 3. ELECTRICAL CHARACTERISTICS OF HIGH-ENERGY
IMPLANTED THERMALLY ANNEALED GaAs SAMPLES

A. Multiple Implants

Wafer No.	Implant Energy (keV)	Implant Dose (cm^{-2})	Carrier Concentration Nm (cm^{-3})	Average Mobility (cm^2/V-s)	Activation Efficiency (%)
H51	70-1000	1.7-7x10^{12}	1.57x10^{17}	4450	81
H52	70-1000	1.7-7x10^{12}	2.09x10^{17}	3990	107
H53	70-1000	40-7x10^{12}	(n$^+$-n)	3050	43
H62	80-900	1.6-7.2x10^{12}	1.96x10^{17}	3850	104
H63	80-900	1.6-7.2x10^{12}	1.85x10^{17}	3960	98

B. Single Implants

Wafer No.	Implant Energy (keV)	Implant Dose (cm^{-2})	Carrier Concentration Nm (cm^{-3})	Average Mobility (cm^2/V-s)	Activation Efficiency (%)
H36	1000	1.5x10^{13}	1.6x10^{17}	4720	53
H37	1000	1.0x10^{13}	2.0x10^{17}	4530	100
H38	1000	1x10^{15}	1.26x10^{18}	1830	6.3
H39	1000	3x10^{15}	7.14x10^{17}	2120	1.2
H50	600	3x10^{15}	7.74x10^{17}	1880	1.2

The implant parameters for wafers H51, H52, and H53 were shown previously in Table 1, and the implant parameters and conditions for wafers H62 and H63 are shown in Tables 4 and 5, respectively; the corresponding calculated Si distribution and measured carrier concentration and mobility profiles of H62 are shown in Fig. 8. Carrier concentration profiles measured using both differential C-V and van der Pauw measurements are included. These last two wafers (H62 and H63) used implant energies for a better approximation of a ~1-μm flat profile. This was made possible by operating the Van de Graaff

TABLE 4. CALCULATED MULTIPLE IMPLANT PARAMETERS FOR FLAT
PROFILES OF Si IN GaAs (WAFERS H62 AND H63)

Energy (keV)	Dose (cm^{-2})
80	1.6×10^{12}
265	4.3×10^{12}
500	5.8×10^{12}
900	7.2×10^{12}

TABLE 5. IMPLANT CONDITIONS FOR WAFERS H62 AND H63

Energy (keV)	80	265	500	900
N_{dose} (cm^{-2})	1.6×10^{12}	4.3×10^{12}	5.8×10^{12}	7.2×10^{12}
Dose No.	31.0	27.7	20.2	25.1
Scale	2×10^{-7}	6×10^{-7}	6×10^{-7}	6×10^{-7}

Area = 24.19 cm^2 Area = 13.07 cm^2

machine at lower energies. Test runs of Si implant in GaAs were made using
the Van de Graaff machine at energies as low as 300 keV. This would eliminate
the dip in the implant profiles encountered previously; it occurred as a result
of lacking energy source in the 300- to 500-keV range due to limitations of the
two implanters used.

The five wafers (H36-H39, H50) listed in Table 3-B were single-dose
implanted at 1000 and 600 keV, respectively. The carrier concentrations for
single-implanted samples were calculated from

$$N_m = N_s / \sqrt{2\pi} \Delta R_p$$

where N_s is the measured sheet carrier concentration, and ΔR_p is the straggle
determined from SIMS profiling (Fig. 2); the ΔR_p's are 0.2 μm at 1000 keV and
0.18 μm at 600 keV.

Single and multiple implantation studies were also carried out at im-
plant energies below 300 keV for optimization of doping profiles of the
implanted n-layers for device (FETs) fabrication, and also for characterization
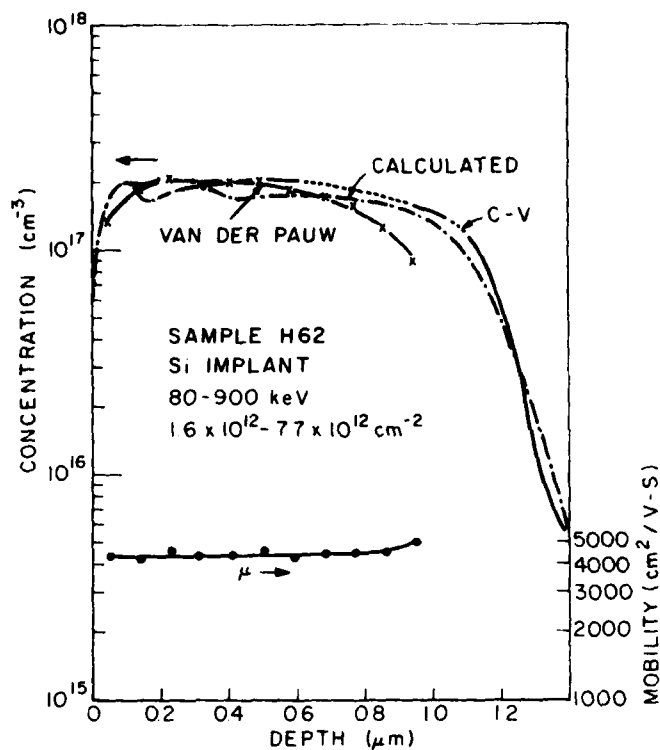
Figure 8. Multiple-implant profiles of H62: calculated
and measured. Mobility profile also included.

of SI GaAs substrates (purchased from different vendors). High-performance
power FETs operating up to 26 GHz were fabricated (in a concurrent program)
from a GaAs wafer made by double Si implantation into SI GaAs substrates fol-
lowed by capless thermal annealing. Power output of ∿220 mW at 15 GHz was
obtained from a single cell (600-μm gate width) with corresponding gain of 6
dB and power-added efficiency of 27%. The power output and efficiency at
26 GHz are 60 mW and 5%, respectively.

The electron density profiles of representative double Si-implanted
thermally annealed samples are shown in Figs. 9 and 10. The profiles were
measured by differential C-V technique combined with controlled chemical etch-
ing [1]. The wafers were capless annealed under arsenic overpressure at 825°C
for 20 min.

Wafers C77 and C77F, shown in Fig. 10, are identical, except that during
annealing two pieces of wafers marked C77F were placed face-to-face on a
carrier in the open quartz tube, while wafer C77 was placed face-up in the
normal way on a carrier in the same open quartz tube. The wafers annealed
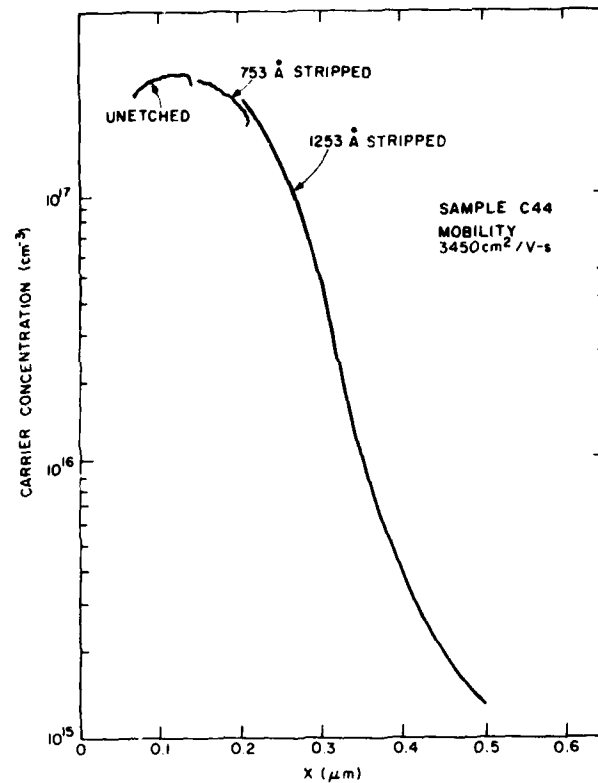
Figure 9. Electron density profile of double-implanted GaAs sample C44.
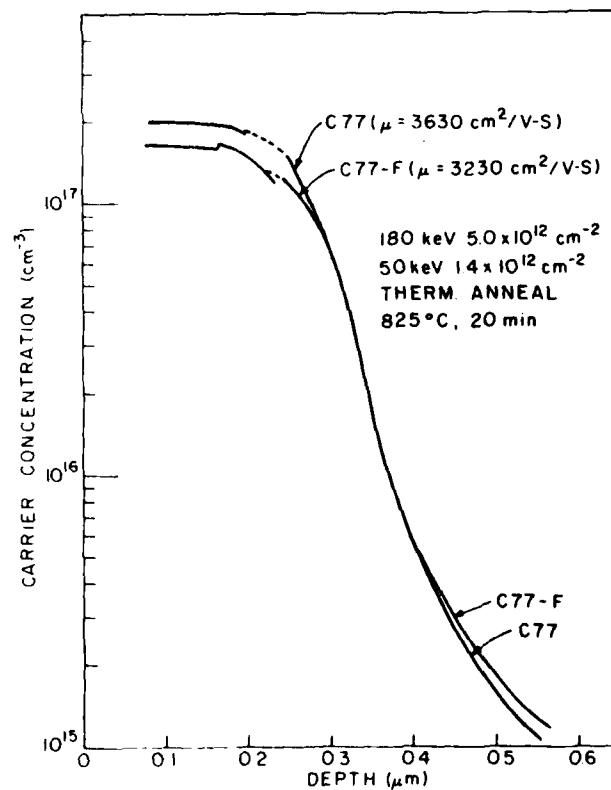
Figure 10. Electron density profiles of double-implanted GaAs
samples. C77F is "face-to-face" annealed.

15

under face-to-face conditions showed lower mobility and activation efficiency, as indicated in Fig. 10. The measured peak carrier concentration density is 1.6×10^{17} cm^{-3} for wafer C77F, and 2.0×10^{17} cm^{-3} for wafer C77. The lower activation and mobility in the face-to-face annealed wafer indicate that the arsenic overpressure system which we used for thermal annealing is superior. It has been reported in the literature that face-to-face annealing has resulted in good quality n-layers.

E.   CAPLESS ANNEALING

Our previous work on capless annealing of implanted GaAs under arsenic overpressure was carried out at 800 to 850°C. Studies were continued on annealing Si-implanted GaAs under different temperatures keeping arsenic overpressure almost constant. The arsenic partial pressure [7] was controlled by varying the flow rate of the AsH_3/H_2 mixture passing through the annealing furnace. .

In the initial experiment, three samples implanted at 200 keV with different doses (2.5×10^{13}, 2.5×10^{14}, and 3×10^{15} cm^{-2}) were annealed at 900°C. The results are shown in Fig. 11, which also includes our previous work on thermal and laser annealing (1979 Annual Report, Fig. 37). Figure 11 shows that the 900°C capless annealing gives rise to electrical activations higher than those of 825°C capless annealed. The measured mobilities of the three 900°C annealed samples were 3030, 1900, and 1740 cm^2/V-s, in the order of increasing carrier concentration. The corresponding compensation factors are 1.1, 1.8, and 1.9, respectively.

Table 6 lists the electrical properties of multiple-implanted samples which were capless annealed under different conditions. The multiple-implant conditions of each wafer are listed in the second column. Note that in high-dose implanted wafers (C71, C72), the sheet resistance of a sample annealed at 900°C is about 60 $\Omega/\square$, which is half that annealed at 825°C. In low-dose implanted wafers (H58, H59), the sheet resistance does not change significantly at these two temperatures. An increase of ~50% in arsenic overpressure at 900°C reduces the sheet resistance about 8% in the low-dose multiple-implanted sample under this high arsenic overpressure condition.

7.   J. R. Arthur, "Vapor Pressures and Phase Equilibria in the GaAs System," J. Phys. Chem. Solids $\underline{28}$, 2257 (1967).
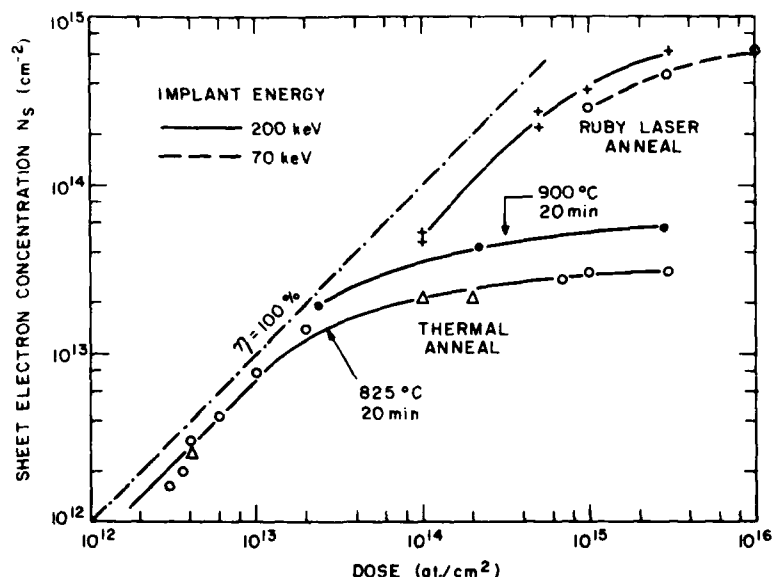
Figure 11. Sheet electron concentration as a function of dose for ruby-laser and thermal-annealed samples.

Further profiling measurements show that the lower sheet resistance is due to the higher carrier concentration in 900°C annealed samples. The depths of the n-layers and the mobilities were approximately the same for both the low (825°C) and high (900°C) temperature annealed samples. These results are indicated in Figs. 12 and 13, which show the electron concentration and mobility profiles of wafer C71 annealed at 825°C and 900°C, respectively.

F. CO-IMPLANT OF ^{28}Si AND ^{32}S IN GaAs

Co-implant of ^{28}Si and ^{32}S at 200 keV into SI GaAs in an attempt to fabricate a high-quality n-layer was investigated. The idea is that while the ^{32}S of column VI occupies the As lattice sites, the amphoteric Si is more readily located in the Ga sites as dopants and hence enhances electrical activation which should result in high-quality doped layers.

Preliminary experiments have shown some encouraging results. First, the electron density profile of a wafer co-implanted with ^{28}Si and ^{32}S at a single energy shows a broader peak similar to dual-energy silicon-implanted GaAs. Second, higher activation efficiency and mobility were measured after the co-implanted wafer was annealed at a higher temperature; this is not observed normally in Si-implanted GaAs at similar low-dose levels.

17

TABLE 6.   ELECTRICAL PROPERTIES OF SI IMPLANTS CAPLESS
ANNEALED UNDER DIFFERENT CONDITIONS

Sample No.	Implant Conditions cm^{-2}	keV	Temp. (°C)	Time (min)	AsH_3 Pressure* (Torr)	Mobility $\mu(cm^2/V\text{-}s)$	Sheet Resistance $Rs(\Omega/\square)$
C70	2×10^{14}	250	825	20	2.0	1760	94
	1×10^{14}	70	900	15	21.3	1690	74
C71	3×10^{15}	200	825	20	2.0	1650	125
	1×10^{15}	70	900	15	21.3	1690	59
C72	1×10^{15}	200	825	20	2.0	1790	124
	5×10^{14}	70	900	15	21.3	1540	55
	7.2×10^{12}	900	825	20	2.0	3860	75
	5.8×10^{12}	500	900	15	21.3	3720	77
H58	4.3×10^{12}	265	900	15	31.9	3760	72
	1.6×10^{12}	80					
	7.2×10^{12}	900	825	20	2.0	3510	71
	5.8×10^{12}	500	900	15	21.3	3880	71
H59	4.3×10^{12}	265	900	15	31.9	3870	74
	1.6×10^{12}	80					

*Actual AsH_3 partial pressure. Since the equilibrium partial pressure
of As over GaAs is an order of magnitude higher at 900°C than at 825°C,
the overpressure is almost constant.

The experiments were performed by co-implant of ^{28}Si and ^{32}S into SI GaAs
substrate at an energy of 200 keV. The implanted doses for ^{28}Si and ^{32}S were
4.5×10^{12} cm^{-2} and 2.3×10^{12} cm^{-2}, respectively. Figure 14 shows the electron
density profiles of the co-implanted sample annealed at 825°C for 20 min and
900°C for 15 min. The activation efficiency increased from 63.2 to 83.8% and
the mobility increased from 3490 to 3910 $cm^2/V\text{-}s$ as the annealing temperature
is increased from 825°C to 900°C. The AsH_3 flow rate is increased more than

18
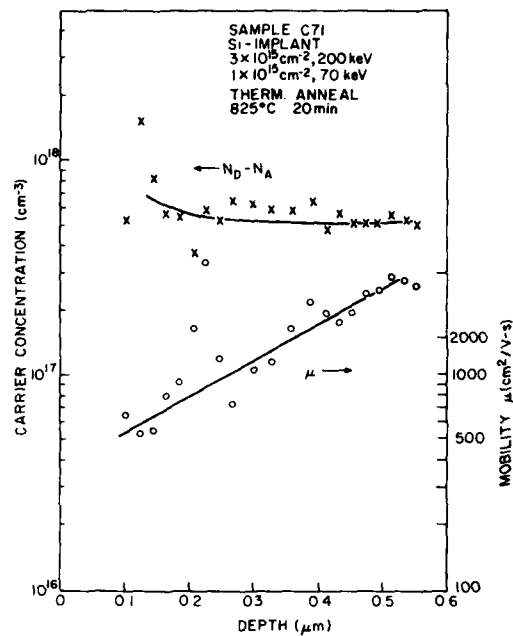
Figure 12.   Carrier concentration and mobility profiles
of C71 annealed at 825°C.
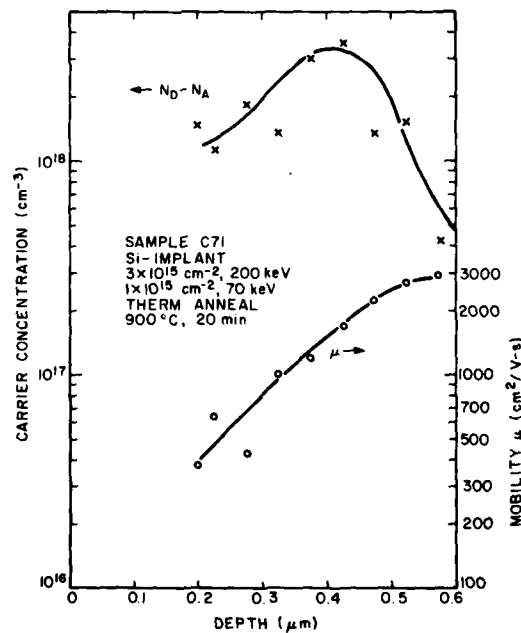
Figure 13.   Carrier concentration and mobility profiles
of C71 annealed at 900°C.

ten times [7] for capless annealing at 900°C to maintain a constant arsenic overpressure the same as that at 825°C. Electron density profiles of Si-implanted and S-implanted GaAs samples which are thermally annealed at 825°C are also included in Fig. 14 as references; both are implanted at 200 keV with doses of 3.5×10^{12} cm^{-2} for Si and 4.5×10^{12} cm^{-2} for S implant. The corresponding mobilities are 3060 and 3900 cm^2/V-s, respectively. Note that the implant energies are the same, but the doses do not equal those in the co-implanted sample. The profiles are included to show the shape of each electron density distribution.
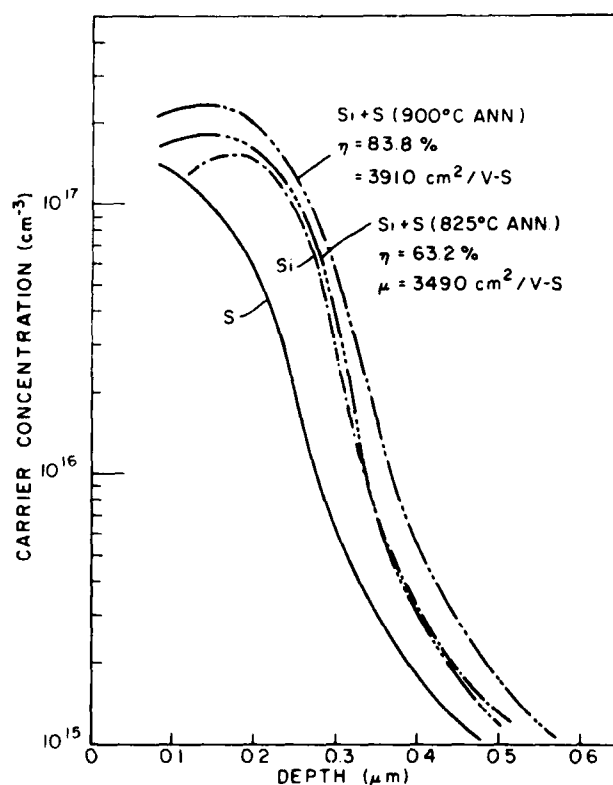
Figure 14. Electron density profiles of co-implanted (^{28}Si and ^{32}S) GaAs annealed at 825 and 900°C, respectively. Individual implants annealed at 825°C are also shown.

The Si implant has a near Gaussian electron density profile indicating a very small thermal diffusion coefficient which has been determined previously [1,2] to be $\leq 10^{-15}$ cm^2/s. The S implant has an electron density profile which increases toward the surface and is considerably deviated from Gaussian. The

electron density profiles of the co-implanted wafer show a broader peak with higher activation and mobility when annealed at higher temperature. These results are encouraging from a device point of view. The mechanisms are not fully understood. Investigations will be continued.

G. Si IMPLANTATION INTO Ar-IMPLANTED SI GaAs SUBSTRATES - IMPROVEMENT OF LOW-DOSE THRESHOLD

Implantation of Si into SI GaAs substrates exhibits a low dose threshold [1,2]; below that threshold, the implanted layer either shows no electrical activation or shows activation with very poor mobility after the implanted wafer is thermally annealed. The dose threshold depends on the substrate material and is typically $\sim 1-2 \times 10^{12}$ cm^{-2} at an implant energy of 200 keV [1,2] which corresponds to an impurity concentration peak of

$$N_m = \frac{N}{\sqrt{2\pi} \, \Delta R_p} \sim 4-8 \times 10^{16} \text{cm}^{-3}$$

This concentration value is of the same magnitude of the Cr concentration in most Cr-doped semi-insulating material used. It is therefore suspected that the amount of Cr concentration or other impurities that are present in the substrate may be related to the dose threshold.

To find out more about the dose threshold dependence, if any, on the chromium contents of the SI GaAs substrate, investigations were made using substrates with different amounts of Cr content. Since Ar implantation in GaAs substrates followed by annealing can redistribute Cr in the substrates without activating the SI GaAs, and since the amount of Cr redistribution is dependent on the doses implanted (details in Section IV), we have therefore used these Ar-treated substrates to investigate the dependence of threshold dose of donor (e.g., Si) upon Cr concentration. Preliminary experiments have shown *extremely interesting* results.

Low dose (2×10^{12} cm^{-2}, 200 keV) Si implantations were made into five Ar-implanted, capless-annealed (825°C, 20 min) SI GaAs samples which were cut from the same SI GaAs substrate. The (100) Cr-doped substrate has a normal low dose threshold of 2×10^{12} cm^{-2}. The fluences of Ar implants varied between 5×10^{12} cm^{-2} and 1×10^{15} cm^{-2}, and the implantations were made at 750 keV using the Van de Graaff machine. High energy is used to effect the Cr redistribution to a greater depth.

21

After capless annealing, three of the Si-implanted samples were activated with mobilities of greater than 4000 cm^2/V-s, as shown in Table 7. The other two samples, which received high-dose Ar implants ($1x10^{14}$ and $1x10^{15}$ cm^{-2}) did not activate. Instead, a conductive layer, which is an indication of conversion, was measured on the surface of one of the wafers ($1x10^{15}$ cm^{-2} implanted). Figures 15, 16, and 17 show the electron density profiles measured by differential C-V on these three electrically activated samples. Each profile shows a normal near-Gaussian distribution with electron density peaks at $6-8x10^{16}$ cm^{-3} and becomes lower toward the surface.

TABLE 7. LOW DOSE ($2x10^{12}$ cm^{-2}, 200 keV) Si IMPLANT
INTO Ar-TREATED SI GaAs SUBSTRATES

Sample	Ar Dose (cm^{-2}) at 750 keV	Mobility (cm^2/V-s)	Activation (%)
R5	$5x10^{12}$	4410	67.4
R6	$1x10^{13}$	4010	74.5
R7	$5x10^{13}$	4080	41.0

The activation of low-dose Si implant in this experiment appears related to the Cr concentration in the Ar-treated substrates. The sample R7, for example, which showed low-dose activation with good mobility and electron density profile, had a reduction in Cr concentration to $\sim10^{16}$ cm^{-3} at a depth of ~0.4 μm near the sample surface. Sample R9, which did not activate, had a Cr peak below the surface to a depth of ~1000 Å, followed by a broad depletion of Cr down to $\sim3x10^{15}$ cm^{-3}. The large amount of chromium depletion is believed to cause the thermal conversion, that is, the presence of a conductive layer on the surface after thermal annealing; because the reduced chromium concentration fails to compensate the background impurities in the substrate. The chromium redistribution profiles will be presented in Section IV.
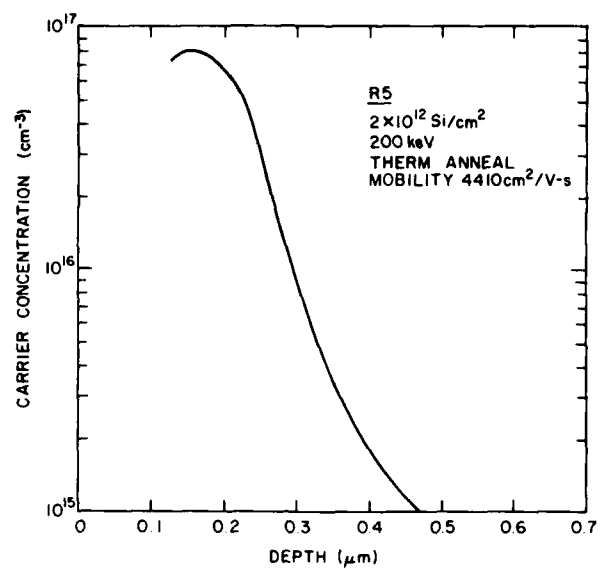
Figure 15.   Electron density profile of R5.
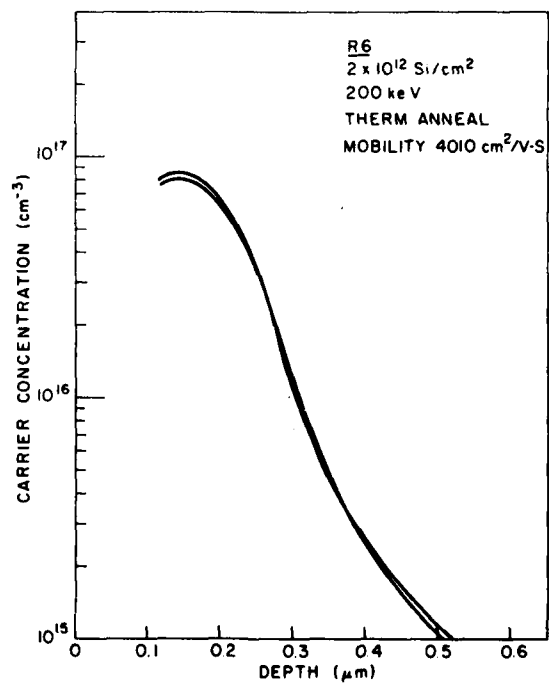
Figure 16.   Electron density profile of R6.
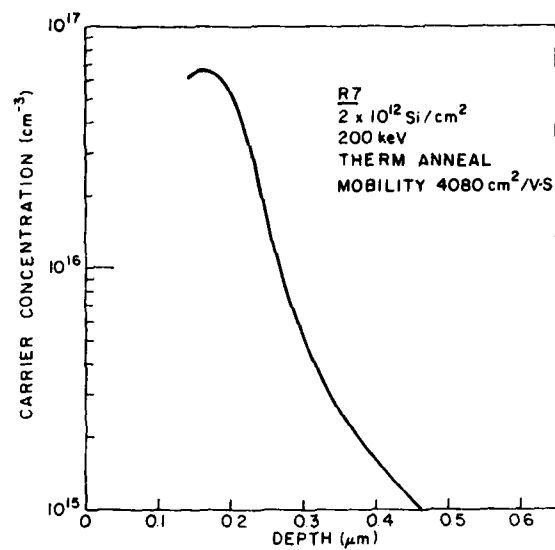
Figure 17.   Electron density profile of R7.

LASER AND ELECTRON BEAM ANNEALING

A. INTRODUCTION

We have previously investigated annealing of Si-implanted SI GaAs using pulsed Nd:Glass [8] and ruby lasers [9]. During this reporting period, laser annealing studies were extended to MeV-implanted GaAs. Sources other than Nd:Glass and ruby lasers were included in the annealing experiments. Other annealing sources being investigated were: a scan pulsed laser beam, a pulsed electron beam, and a pulsed dual-frequency laser beam.

In this section we will describe the electrical properties and surface morphologies of laser (or electron beam) irradiated GaAs. Preliminary results on crystallinity of laser (or electron beam) irradiated GaAs will also be described.

B. ANNEALING Si-IMPLANTED GaAs USING LASER-BEAM IRRADIATION

1. Q-Switched Ruby Laser

The semi-insulating [100] GaAs substrates were implanted with Si at energies between 70 and 200 keV and fluences between 1×10^{14} and 1×10^{16} cm^{-2}. The implanted wafers were cleaved into samples 0.5 to 2 cm^2, and annealing experiments were carried out with single laser-beam pulses in air with no encapsulation on the samples. The Q-switched ruby laser was operated with an output energy density of between 0.2 and 2.3 J/cm^2 per pulse (30 ns FWHM). The laser beam irradiates an area of approximately 10 cm^2 after passing through a lens. The energy density of the laser output pulse was measured with a calibrated (+5%) ballistic thermopile.

Tables 8 and 9 summarize electrical properties of 200 keV and 70 keV Si-implanted ruby-laser-irradiated GaAs compared with similar samples annealed thermally. These data were obtained from van der Pauw measurements and were tabulated in terms of sheet resistance ρ_2, mobility μ, and activation efficiency

8. S. G. Liu, C. P. Wu and C. W. Magee, "Annealing of Ion-Implanted GaAs with Nd:Glass Laser," AIP Conference Proceedings, No. 50, 603 (1978).
9. S. G. Liu, C. P. Wu and C. W. Magee, "Annealing of Ion-Implanted GaAs with a Pulsed Ruby Laser," Symposium Proceedings on Laser and Electron Beam Processing of Materials, Academic Press, 341 (1980).

TABLE 8. ELECTRICAL PROPERTIES OF 200-keV Si-IMPLANTED
RUBY-LASER-IRRADIATED GaAs

Si Implantation		Ruby Laser Annealing				Thermal Annealing		
Energy (keV)	Dose (cm^{-2})	E (J/cm^2)	ρ_s ($\Omega/\square$)	μ (cm^2/V-s)	η (%)	ρ_s ($\Omega/\square$)	μ (cm^2/V-s)	η (%)
200	1×10^{14}	2.3	104	1300	46.3			
200	1×10^{14}	1.7	91	1350	51.0	132	2200	21.5
200	1×10^{14}	0.6	1600	454	8.6			
200	5×10^{14}	2.3	27	1030	45.5			
200	5×10^{14}	1.7	27	830	55.6	112	1738	6.4
200	5×10^{14}	1.0	320	280	14.0			
200	3×10^{15}	2.3	27	370	20.8			
200	3×10^{15}	1.8	31	355	18.9	130	1938	0.8
200	3×10^{15}	1.0	57	250	14.5			

TABLE 9. ELECTRICAL PROPERTIES OF 70-keV Si-IMPLANTED
RUBY-LASER-IRRADIATED GaAs

Si Implantation		Ruby Laser Annealing				Thermal Annealing		
Energy (keV)	Dose (cm^{-2})	E (J/cm^2)	ρ_s ($\Omega/\square$)	μ (cm^2/V-s)	η (%)	ρ_s ($\Omega/\square$)	μ (cm^2/V-s)	η (%)
70	1×10^{15}	2.3	39	693	23.0			
70	1×10^{15}	1.7	29	745	29.4	170	1712	2.1
70	1×10^{15}	0.8	156	314	12.8			
70	3×10^{15}	2.3	24	564	15.1			
70	3×10^{15}	1.7	29	496	14.6			
70	3×10^{15}	1.3	52	300	13.3	72	1387	2.1
70	3×10^{15}	0.8	148	172	8.2			
70	1×10^{16}	2.3	21	481	6.3			
70	1×10^{16}	1.3	93	210	3.2	90	1727	0.4

η, which is defined as the ratio of the electrically activated sheet carrier concentration N_s to the implanted fluence. The thermal annealing was carried out under arsenic overpressure at 825°C for 20 minutes. The higher activation efficiency of 200-keV implants rather than that of 70-keV implants at a given fluence is believed due to the lower atomic Si concentration associated with the broader straggle of 200-keV implants.

Tables 8 and 9 show that the activation efficiency and hence the sheet carrier concentration is considerably higher in laser-irradiated samples than it is in thermally annealed samples. The mobility of laser-irradiated GaAs, however, is lower than that of thermally annealed samples, even taking into consideration the expected lower mobility as a result of higher carrier density. The net effect of a much higher activation and a lower mobility results in a lower sheet resistance in high-energy laser-irradiated GaAs as shown in Tables 8 and 9.

The atomic profiles of high-dose implanted laser-irradiated GaAs were investigated previously. The amount of impurity profile broadening depends on the energy density of the laser beam. A substantial broadening was observed in samples irradiated with a high energy density beam. The SIMS profile of a 1 J/cm^2 pulsed ruby laser irradiated GaAs (3×10^{15} cm^{-2}, 200 keV implanted) shows no significant broadening as compared with profiles of the as-implanted and the thermally annealed samples (Fig. 18). The same sample, however, has shown high electrical activation (Table 8). This result indicates that under proper conditions, Si-implanted GaAs can be electrically activated using a pulsed laser beam without melting the implanted layer. Rapid diffusion in a liquid state has been regarded [10] as the cause for substantial impurity profile broadening observed in ion-implanted laser-annealed silicon.

2. Q-Switched Nd:Glass Laser

The photon energy of the Nd:Glass laser of 1.17 eV (λ = 1.06 μm) is lower than the bandgap of GaAs (1.4 eV at 300 K). The optical absorption at 1.06 μm is therefore dependent upon the amount of impurities and lattice defects produced by implantation. The Nd:Glass laser may therefore be suitable for deep impurity distribution such as that which is produced by MeV Si implantation in GaAs.

Annealing of high-energy (>600 keV) Si-implanted GaAs wafers was investigated using a high-power pulsed Nd:Glass laser. The electrical characteristics were evaluated using van der Pauw measurements. The results are tabulated in Table 10. Two samples were single-energy implanted and two were multiple implanted. The multiple-implanted samples (N6A, N6B) were implanted using five energies between 40 and 900 keV with corresponding fluences between

10. J. C. Wang, R. F. Wood and P. P. Pronko, "Theoretical Analysis of Thermal and Mass Transport in Ion-Implanted Laser-Annealed Silicon," Appl. Phys. Lett. 33, 445 (1978).

$Si \rightarrow GaAs, A82, 200\,keV, 3\times10^{15}\,at/cm^2$

THERMALLY ANNEALED

UNANNEALED

LASER ANNEALED $(1.0\,J/cm^2)$
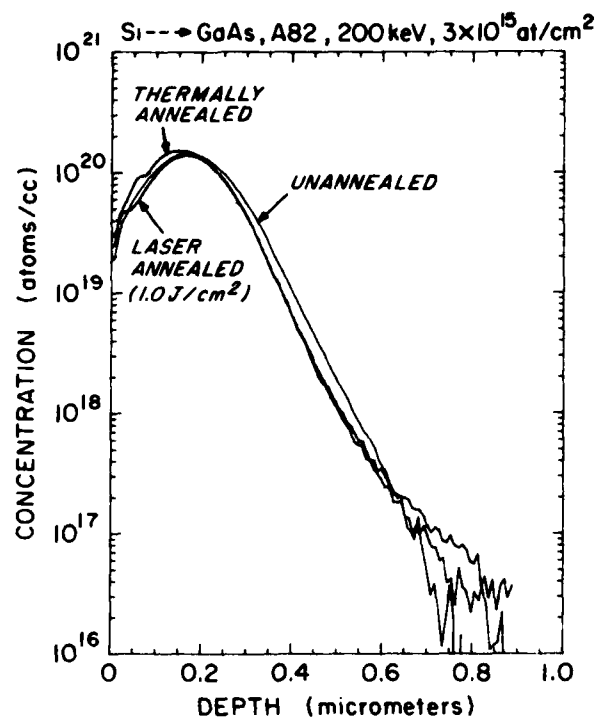
Figure 18.   SIMS profiles showing Si-implanted GaAs which are (i)
as-implanted, (ii) 1.0 J/cm^2 and ruby-laser irradiated,
and (iii) thermal annealed.

TABLE 10.   ELECTRICAL PROPERTIES OF HIGH-ENERGY Si-
IMPLANTED Nd:GLASS-LASER-IRRADIATED GaAs

Sample No. (Implant No.)	Impl. Energy (keV)	Impl. Dose (cm^{-2})	Laser Energy (J/cm^2)	N_s (cm^{-2})	μ $(cm^2/V\text{-}s)$	ρ_s $(\Omega/\square)$	η (%)
N7(H7)	600	2.52×10^{15}	1.5	7.88×10^{13}	734	108.0	3.1
N8(H8)	700	2.70×10^{15}	1.5	2.23×10^{14}	1027	27.0	8.2
N6A(H24)	40 to 900	1.41×10^{14} to 1.30×10^{15}	1.5	7.14×10^{14}	488	17.9	22.0
N6B(H24)	40 to 900	1.41×10^{14} to 1.30×10^{15}	1.2	3.58×10^{14}	464	37.6	11.0

1.41×10^{14} and 1.30×10^{15} cm^{-2}, and were designed to produce a uniform 1-μm silicon concentration of $1/3 \times 10^{20}$ cm^{-3}. The fact that high-energy implanted samples can be activated with the irradiation of an Nd:Glass laser is encouraging.

Figures 19 and 20 show the depth distribution of carrier density and mobility of the multiple-implanted samples, N6A and N6B, respectively. The samples were evaluated using differential van der Pauw measurements. The measurements show that the carrier density reached $\sim 2 \times 10^{19}$ (N6A) and $\sim 9 \times 10^{18}$ (N6B) at 1-μm depth below the sample surface. The corresponding mobilities were ~ 300 cm^2/V-s. Much lower carrier concentrations with higher mobilities were measured toward the sample surface. The significance of the depth profile of carrier concentrations and mobilities is that pulsed Nd:Glass laser beams can be used to activate 1-μm-deep MeV implanted GaAs. The lower carrier concentration at the sample surface may be related to (i) the lower dose at the low energy end of the multiple implants and (ii) the decrease in carrier concentration in laser-irradiated GaAs following a subsequent thermal treatment [11]. Ohmic contacts for differential van der Pauw measurements were formed at an elevated temperature of 450°C for 1 min. The carrier concentration can decrease substantially at sample surfaces [11] when high-dose implanted laser-irradiated GaAs is subsequently thermally treated at this temperature. The electron density profiles of laser-irradiated implants will be further studied to clarify the possible discrepancies in the measured electron density profiles due to low-temperature thermal treatment.

3. Q-Switched Nd:Glass with Frequency Doubler

Annealing of high-dose implanted GaAs samples was studied using a double-frequency laser beam (Nd:Glass laser, $\lambda=1.06$ μm, with a doubler, $\lambda=0.53$ μm). The output power of the doubler is 15% of the total power. The samples irradiated with double-frequency laser beam show good surface morphology at irradiated energy densities of 0.9 to 1.2 J/cm^2. Nonalloyed ohmic contacts with Ti/Pt/Au metallization were successfully made onto the double-frequency laser-irradiated surface. Table 11 shows the electrical properties measured by van der Pauw measurements on samples implanted with different doses and irradiated with laser beams at different energy densities.
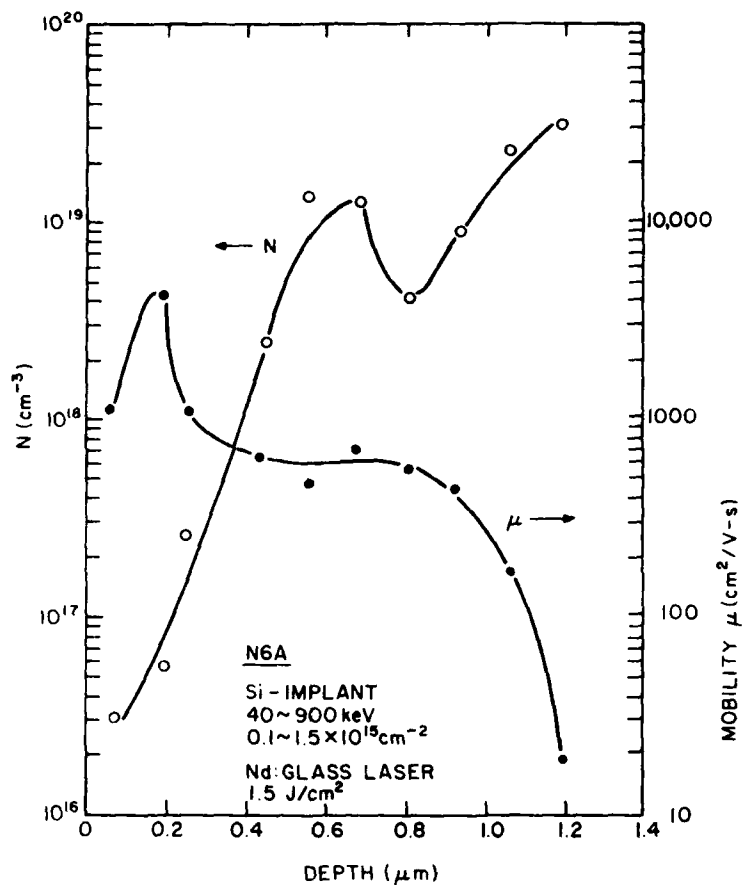
Figure 19. Depth distribution of carrier concentration and mobility of multiple-implanted GaAs; laser irradiated at 1.5 J/cm^2.

C. ANNEALING Si-IMPLANTED GaAs USING ELECTRON BEAM OR SCAN PULSED LASER BEAM

Annealing of implanted GaAs samples was studied using sources other than single-pulse high-power Q-switched lasers. The annealing systems being studied were: (1) a scan pulsed laser with a wavelength of 0.53 μm and (2) a pulsed electron beam system. Annealing experiments with the 0.53-μm laser were performed using the Quantronix Corporation (Smithtown, NY) Model 610 Epitherm which is a Q-switched Nd:YAG laser with a second harmonic generator. The laser pulse width is 100 ns, repetition rate is 7 kHz, and beam spot size is ∿5 mil in diameter. The pulsed electron beam experiments were carried out at Spire Corporation, Bedford, MA. The pulse width is 100 ns, and each sample is annealed with a single pulse.

30
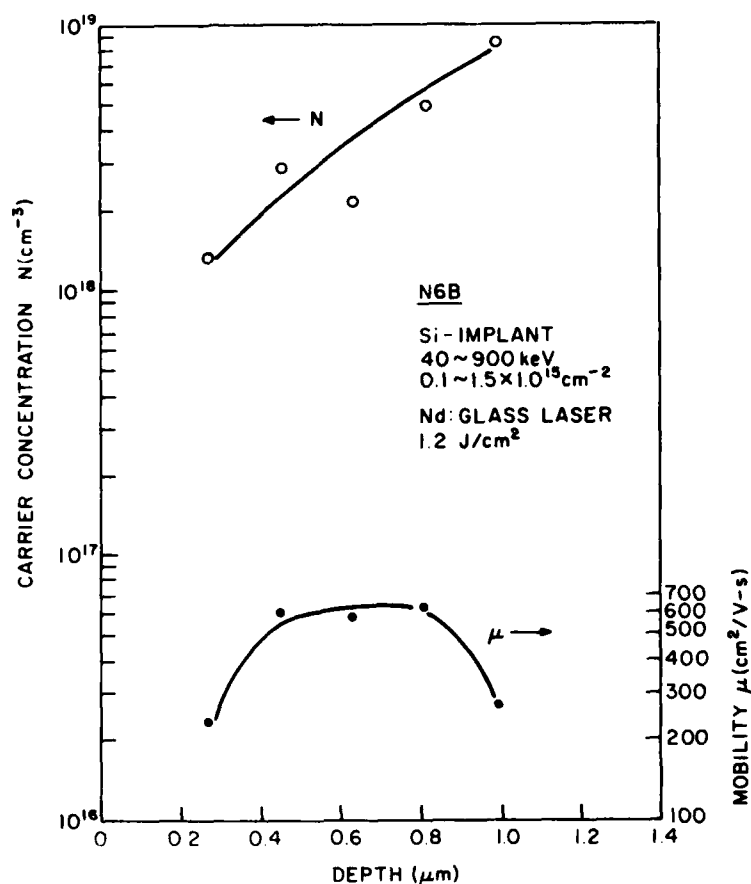
Figure 20. Depth distribution of carrier concentration and mobility of multiple-implanted; GaAs laser irradiated at 1.2 J/cm^2.

Preliminary results on scan-laser experiments using an energy density of 1.8 J/cm^2 were not very encouraging. All samples showed scan marks on the surface which may be an indication of dissociation at the surface. Probing the surface showed no activation except for one sample which has light scanning marks. After cleaning in HCl, that sample (3×10^{15} cm^{-2}, 70 keV Si-implanted) showed a sheet carrier concentration of 9.1×10^{13} cm^{-2}, a mobility of 479 cm^2/V-s, and a sheet resistance of 144 $\Omega/\square$. A similar sample irradiated with a 1-J/cm^2 pulsed ruby laser had a sheet carrier concentration of 2.9×10^{14} cm^{-2}, a mobility of 273 cm^2/V-s, and a sheet resistance of 77 $\Omega/\square$. The irradiated layer was activated without requiring HCl treatment.

TABLE 11. ELECTRICAL PROPERTIES OF HIGH-DOSE Si-IMPLANTED
GaAs IRRADIATED WITH DUAL-FREQUENCY LASER BEAM

Sample	Implant Energy (keV)	Dose (cm^{-3})	Laser Energy $E(J/cm^{-2})$	Sheet Resistance R_s ($\Omega/\square$)	Mobility $\mu(cm^2/V\text{-}s)$	Activation η (%)
L-16	200	$3x10^{15}$	1.2	24.8	403	15.6
	70	$1x10^{15}$				
L-17	200	$1x10^{15}$	1.2	51.9	442	18.1
	70	$5x10^{14}$				
L-15	250	$2x10^{14}$	1.0	373.0	504	11.0
	70	$1x10^{14}$				
L-19	200	$4x10^{14}$	1.1	168.0	518	14.4
	50	$1x10^{14}$				
L-3	200	$3x10^{15}$	0.88	144.0	247	5.9

Results on samples annealed with pulsed electron beams were quite encouraging. The electrical activation is comparable to that annealed with high-power pulsed laser beams. For example, a $3x10^{15}$ cm^{-2}, 200-keV Si-implanted GaAs sample following electron-beam annealing gave a sheet electron density of $5.6x10^{14}$ cm^{-2}, a sheet resistance of 45 $\Omega/\square$, a mobility of 246 $cm^2/V\text{-}s$, and an activation efficiency of 18.7%. These results are comparable with similar samples irradiated with ~1.2 J/cm^2 pulsed ruby laser. Nonalloyed ohmic contacts were formed by depositing either Ti/Pt/Au or AuGe/Ni/Au on electron-beam irradiated samples.

SIMS profiles on a Si-implanted GaAs sample before and after electron-beam annealing are shown in Fig. 21. A slight redistribution in impurity density is detected. The sample was implanted at 200 keV with a fluence of $3x10^{15}$ cm^{-2}, and irradiated with a 100-ns pulse at 0.7 J/cm^2, at 20 keV.
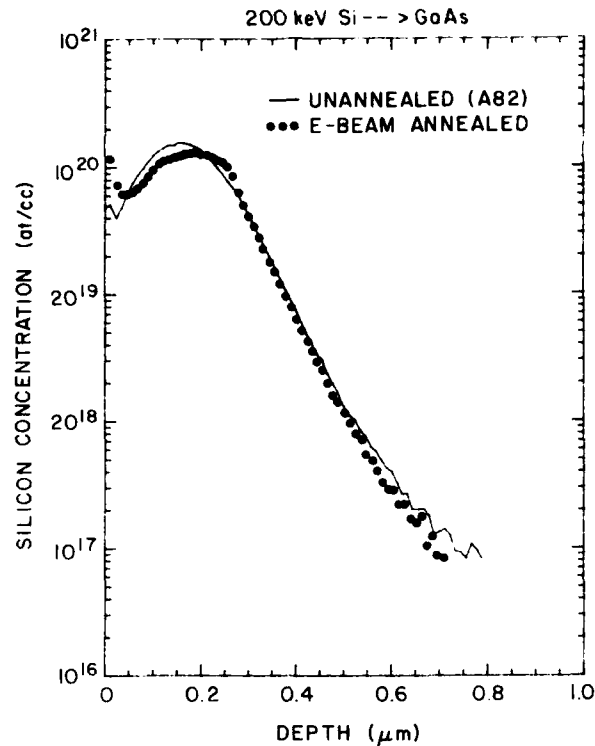
Figure 21. Impurity profiles of Si-implanted GaAs sample before and after electron beam annealing at 0.7 J/cm^2.

D. NONALLOYED OHMIC CONTACTS

To form ohmic contacts on n-type GaAs, a thermal alloying step is normally required after the metal is deposited onto the GaAs surface. Metallizations conventionally used are AuGe/Ni/Au, and alloying is normally done at 400 to 450°C for approximately 1 min. Nonalloyed ohmic contacts on n-GaAs have been reported by evaporation of metal onto high concentration ($\geq 1 \times 10^{19}$ cm^{-3}) n^{++}-GaAs produced by molecular beam epitaxy (MBE) [12], or high fluence implants irradiated by electron [13] or laser [9] beams. Recent developments in ohmic contacts and their correlations with theory were discussed in a paper by Yoder [14].

12. P. A. Barnes and A. Y. Cho, "Nonalloyed Ohmic Contacts to n-GaAs by Molecular Beam Epitaxy," Appl. Phys. Lett. 33, 651 (1978).
13. R. L. Mozzi, W. Fabian and F. J. Piekarcki, "Nonalloyed Ohmic Contacts to N-GaAs by Pulse Electron Beam-Annealed Selenium Implants," Appl. Phys. Lett. 35, 337 (1979).
14. M. N. Yoder, "Ohmic Contacts in GaAs," Solid State Electronics 23, 117 (1980).

We have demonstrated nonalloyed ohmic contacts made by evaporation of AuGe or Ti-Pt-Au directly onto high-dose implanted high-power pulsed-laser or electron-beam-irradiated GaAs. The use of refractory metallization allows one to form ohmic contacts over n^{++} regions, and Schottky contacts over n-regions, concurrently. This may be used to simplify device processing. Not all laser-irradiated GaAs samples are capable of forming nonalloyed ohmic contacts using both AuGe and Ti-Pt-Au metallizations. In a number of Si-implanted GaAs samples irradiated with pulsed ruby laser beams we only succeeded in making nonalloyed ohmic contacts with AuGe-based metallization [9]. This is illustrated in Fig. 22, which shows I-V curves between as-evaporated Ti/Pt/Au and Au-Ge/Ni/Au contact pads on laser-irradiated GaAs, respectively. The reasons are not fully understood. Nonalloyed ohmic contacts using Ti-Pt-Au metallization were made on high-dose implanted GaAs irradiated with dual-frequency laser beam.
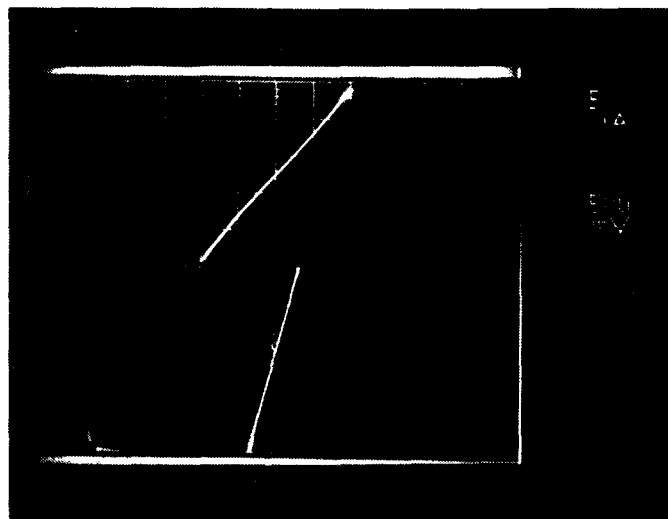
Figure 22. I-V curves between as-evaporated metal contacts (Top: Ti:Pt:Au/500:500:1000 Å; Bottom: AuGe:Ni:Au/1500:500: 2000 Å) on Si-implanted laser-irradiated GaAs.

Table 12 shows electrical performance of nonalloyed ohmic contacts using AuGe based (AuGe/Ni/Au or AuGe/Au) metallization. The sheet resistances, ρ_s, and contact resistivities, ρ_c, were measured by Transmission Line Method (TLM) [15]. The measured resistivities of a number of samples were between 1×10^{-5}

15. H. H. Berger, "Models for Contacts to Planar Device," Solid State Electron. 15, 145 (1972). Also, J. Electrochem. Soc. 119, 507 (1972).

TABLE 12. PERFORMANCE OF NONALLOYED OHMIC CONTACTS USING AuGe-BASED METALLIZATION

Sample	Si-Implant Dose (cm^{-2})	Energy (keV)	Energy Density (Ruby Laser) (J/cm^2)	ρ_s $(\Omega/\square)$	ρ_s 10^{-6} $(\Omega\text{-}cm^2)$
9D	1×10^{15}	70	0.8	~50	~2.6-6.3
7D	3×10^{15}	70	0.8	137-55	~3.5-9.7
104F	3×10^{15}	70	1.0	95-69	~0.3-3.7

and 3×10^{-7} $\Omega\text{-}cm^2$. The corresponding sheet resistance measured was between 50 and 140 $\Omega/\square$. The thickness of the Au-Ge layer was 900 to 1500 Å, and the thickness of the Au layer was 2500 Å. The presence of the Ni layer (300 to 500 Å) did not appear to change the ohmic contact characteristics. Figure 23 shows the Auger analysis (performed by J. H. Thomas of RCA Laboratories) of an AuGe/Ni/Au nonalloyed ohmic contact on GaAs; it shows little interaction between the Ni and other metal layers. It should be pointed out that the 70 keV, high-dose implanted, ruby-laser-irradiated samples showed "hot spots" in some areas on the surface. The measurements were made on metal patterns located in regions free from hot spots.

Table 13 shows electrical performance of nonalloyed ohmic contacts using Ti-Pt-Au metallization. The thickness of each metal layer was Ti, 500 Å, Pt, 500 Å, and Au, 2500 Å. The implanted surfaces were irradiated with a dual-frequency laser beam, the output from a Nd:Glass laser ($\lambda=1.06$ μm) plus that from a frequency doubler made from CD*A crystal.

Sample L16, the multiple implanted dual-frequency laser-beam-irradiated sample, appears to give the best combined nonalloyed ohmic contact performance among the samples tested: low sheet resistance, low contact resistivity and good surface morphology. Figures 24 and 25 show, respectively, Nomarski interference contrast micrographs of sample L16, before and after the evaporation of square Ti-Pt-Au metal patterns. The atomic profiles of L16 were measured by SIMS. There is no significant profile broadening after the sample is irradiated with double-frequency laser beam at 1.2 J/cm^2.
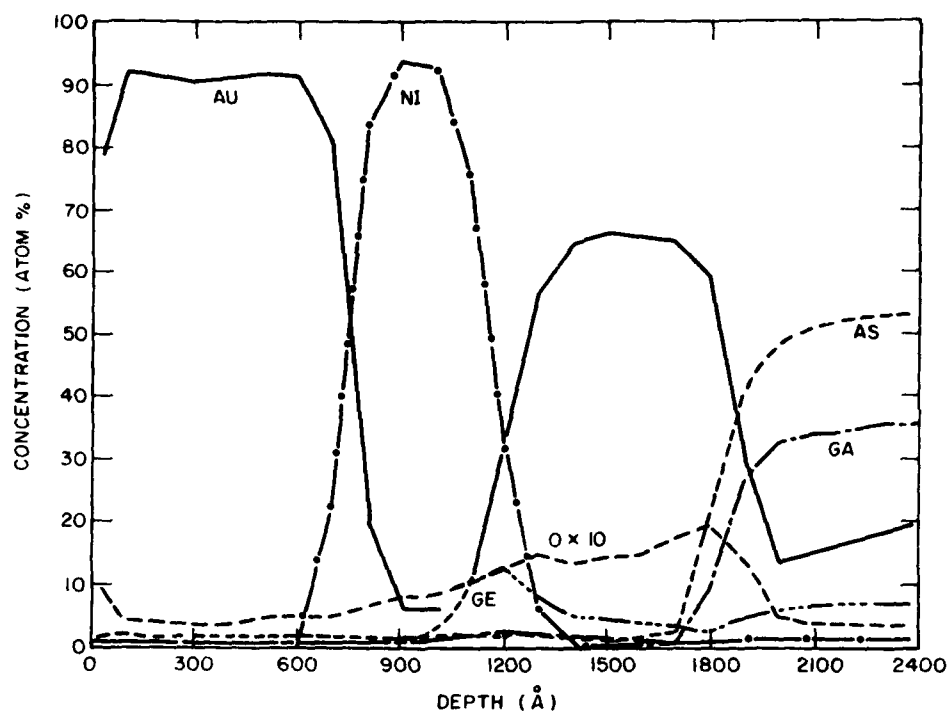
Figure 23. Auger profile of unalloyed AuGe/Ni contacts on laser-annealed sample.

TABLE 13. PERFORMANCE OF NONALLOYED OHMIC CONTACTS USING Ti-Pt-Au METALLIZATION

	Si-Implant		Energy Density		
	Dose	Energy	(Ruby Laser)	ρ_s	ρ_s
Sample	(cm^{-2})	(keV)	(J/cm^2)	$(\Omega/\square)$	$10^{-6} (\Omega\text{-}cm^2)$
L3	3×10^{15}	200	0.88	109-80	39-148
L16	1×10^{15}	70	1.20	35-26	8.7-21
	3×10^{15}	200			

E. SURFACE MORPHOLOGY AND CRYSTALLINITY

In the study of laser annealing of Si-implanted GaAs and the formation of nonalloyed ohmic contacts on these samples, it is desirable to optimize implant parameters and anneal conditions to achieve low sheet resistance, low contact

36

Figure 24. Nomarski interference contrast micrograph of sample
L16; 1.2 J/cm² double-frequency laser irradiated.

Figure 25. Nomarski interference contrast micrograph of nonalloyed
Ti-Pt-Au contact pads on laser irradiated sample L16.
Magnification: 200X.

resistivity, and good surface morphology. The surface morphology and crystal-
linity of laser-irradiated GaAs implants were investigated using the scanning
electron microscopy (SEM) and reflection high-energy electron diffraction

37

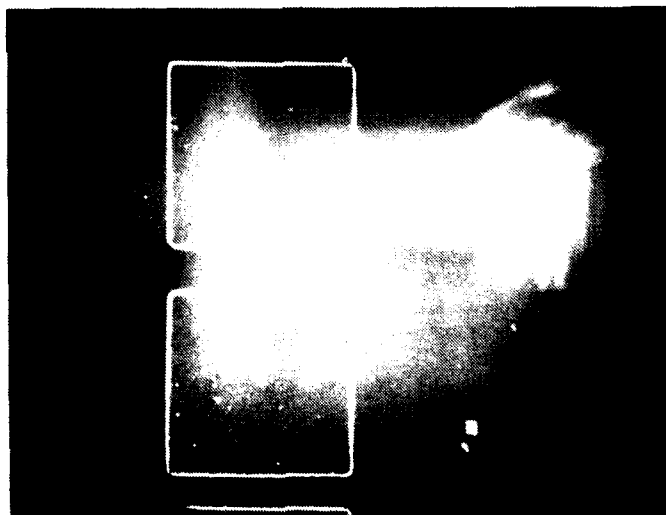(RHEED) analyses*, respectively. Preliminary results showed some correlations between the electrical activation, surface structures, and the crystallinity.

Table 14 lists characteristics of Si-implanted GaAs irradiated with either a laser or an electron beam. The laser beams are either from a ruby laser ($\lambda=0.69$ μm) or a Nd:Glass laser with a frequency doubler ($\lambda=1.06$ and 0.53 μm). Both the laser and electron beam are pulse-operated, as described previously. The sheet resistances are obtained from van der Pauw measurements. The surface structures are referred to those measured using SEM or Nomarski interference contrast micrograph. Table 14 indicates the following correlations between the electrical activation, surface structures, and crystallinities:

1. Under irradiation conditions where the implanted layer turns into single crystal, the sheet resistance is low (24 to 57 $\Omega/\square$) and the SEM shows no structures on the surface [Figs. 26(a) and 26(b)], although the surface in some cases visually shows damaged regions or waviness [1].

2. Under irradiation conditions where the implanted layer turns poly-crystalline, the sheet resistance is high ($\gtrsim 100$ $\Omega/\square$), and the SEM shows microstructures on the surface [Figs. 27(a) and 27(b)] although the surface visually (or viewed with the aid of a Nomarski inter-ference microscope) appears smooth.

Table 14 also shows that nonalloyed ohmic contacts can be formed onto ion-implanted GaAs layers which become polycrystalline after laser or electron beam irradiation; this occurs when either the energy densities of the beams or the implanted impurity concentrations are low. These ohmic contacts will not be very practical because of the high sheet resistances of the non-single-crystal (or small grained) GaAs. Samples such as EB1 (electron-beam-irradiated) or L16 (dual-frequency laser-beam irradiated) shown in Table 14 are more suitable for nonalloyed ohmic contact applications.

Some results on RHEED measurements showing the crystallographic informa-tion are given in Figs. 28(a), (b), and (c). Figure 28(a) shows the result of sample 105F which was annealed using a 1.0 J/cm^2 pulsed ruby laser beam. The dif-fraction from the surface produces a strong, well-formed diffraction pattern of GaAs. The pattern indicates that the surface of the sample is a (100)

---

*The RHEED analyses were made by J. T. McGinn, RCA Laboratories, Princeton, NJ.

TABLE 14. CHARACTERISTICS OF SI-IMPLANTED GaAs IRRADIATED
BY PULSED LASER OR ELECTRON BEAM

Sample	Si-Implant Energy Dose (keV)(cm^{-2})	Crystallinity	Laser or EB Irradiation (J/cm^2)	Sheet Resistance ($\Omega/\square$)	Surface Structure (SEM 20K)
L3*	200 3x10^{15}	Both poly and single crystal	0.88 J/cm^2 (λ=1.06 & 0.53 μm)	144	yes**
105F	200 3x10^{15}	Single crystal	1.0 J/cm^2) (λ=0.69 μm)	57	--
73F	70 3x10^{15}	Single crystal	2.3 J/cm^2 (λ=0.69 μm)	24	not†
7D*	70 3x10^{15}	Broad rings indicating small grained GaAs	0.8 J/cm^2 (λ=0.69 μm)	148	yes**
EB1*	200 3x10^{15}	Single crystal	Elec. Beam 0.7 J/cm^2, 20 keV	45	no**
EB3*	100 1x10^{15}	--	Elec. Beam 0.7 J/cm^2 20 keV	--	yes**
L16*	200 3x10^{15} 70 1x10^{15}	--	(λ=1.06 & 0.53 μm)	25	no**

*nonalloyed ohmic contact formed

**surface visually smooth

†surface visually uneven

plane. Figure 28(b) shows evidence for both poly- and single-crystalline GaAs within 100 Å of the surface for sample L3, which was irradiated with a 0.88-J/cm^2 dual-frequency laser beam (Nd:Glass plus frequency doubler). Figure 28c shows the diffraction pattern of single-crystal surface of an electron-beam-irradiated GaAs. The GaAs samples shown in Figs. 28(a), (b), and (c) were Si-implanted at 200 keV with fluences of 3x10^{15} cm^{-2}.
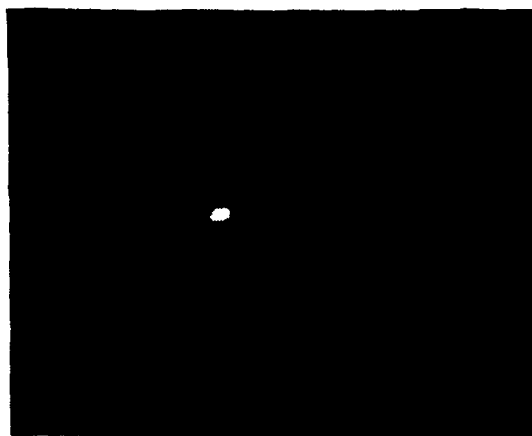
(a)
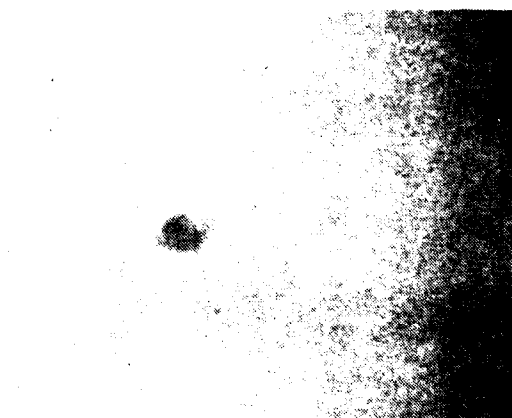
(b)

Figure 26.   (a) SEM (10K, 45°) of Sample 73F; (b) SEM (20K, 50°)
of sample EB1.

(a)

(b)

Figure 27.   (a) SEM (20K, 55°) of sample L3; (b) SEM (20K 55°)
             of sample EB3.

41

(a)

(b)

(c)

Figure 28.   (a) RHEED analysis of 105F, 1.0 J/cm^2 ruby-laser irradiated;
(b) RHEED analysis of L3, 0.88 J/cm^2 dual-frequency, laser
irradiated; (c) RHEED analysis of EB1, 0.7 J/cm^2 electron
beam irradiated.

CHROMIUM REDISTRIBUTION IN GaAs

A. INTRODUCTION
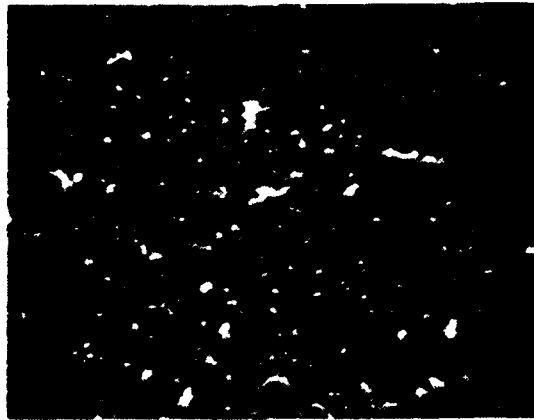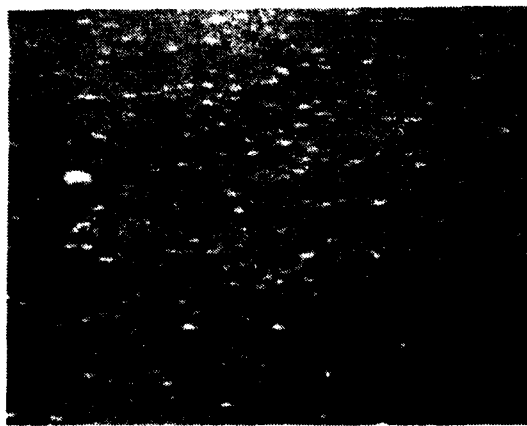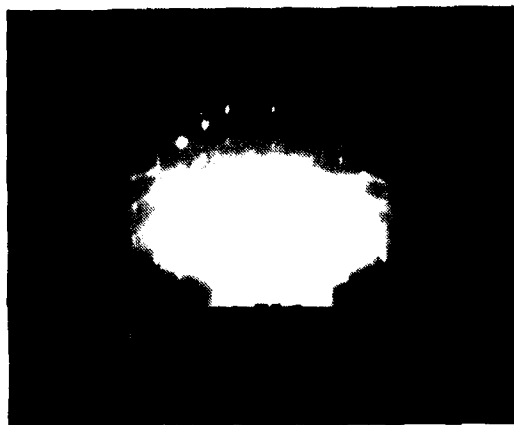
A number of recent publications [16-19] have reported diffusion or re-
distribution of chromium in thermally annealed SI GaAs substrates with or
without implanted impurities. We have studied the dependence of Cr redistri-
bution on fluences [1,2] in thermally annealed SI GaAs substrates which were
implanted with Si at energies of 200 and 600-1000 keV. Similar studies were
made on ^{40}Ar-implanted and thermally annealed GaAs. The implant of ^{40}Ar has
shown similar Cr-redistribution profiles as the ^{28}Si implants. This indicates
that Cr redistribution is caused mainly by implant damage and thermal treat-
ment, because argon is neutral and has no other effect than introducing damage
in the crystal. Argon-treated SI GaAs substrates have shown low dose activa-
tion threshold with good mobility for subsequent silicon implantation, as
described previously in Section III.

B. CHROMIUM DISTRIBUTION IN Si-IMPLANTED GaAs DUE TO IMPLANT AND ANNEAL

Chromium profiles of Si-implanted semi-insulating GaAs were investigated
using SIMS measurements. The SIMS system at RCA is capable of detecting
atomic chromium density of $<5 \times 10^{15}$ cm^{-3}.

Studies on the redistribution of Cr in the SI GaAs substrate due to the
implantation and annealing operations indicate that the redistribution of Cr
is a strong function of implant dose and the annealing method.

Figures 29(a) and (b)* show, respectively, SIMS profiles of low dose (4×10^{12}
cm^{-2}, 200 keV) Si implants before and after the wafers were capless-annealed

16. A. M. Huber, G. Morillot and N. T. Linh, "Chromium Profiles in Semi-
     insulating GaAs after Annealing with a Si$_3$N$_4$ Encapsulant," Appl. Phys.
     Lett. 34, 858 (1979).
17. R. G. Wilson, P. K. Vasuder, D. M. Jamba, C. A. Evans, Jr. and V. R.
     Deline, "Chromium Concentrations, Depth Distributions and Diffusion
     Coefficient in Bulk and Epitaxial GaAs and in Si," Appl. Phys. Lett.
     36, 215 (1980).
18. J. Kasahara and N. Watanabe, "Redistribution of Cr in Capless-Annealed
     GaAs Under Arsenic Pressure," Jap. J. of Appl. Phys. 19, L151 (1980).
19. C. A. Evans, Jr. and V. R. Deline, "Redistribution of Cr During Anneal-
     ing of ^{80}Se-implanted GaAs," Appl. Phys. Lett. 35, 291 (1979).

*SIMS profiles in Fig. 29 were measured by Charles Evans and Associates.
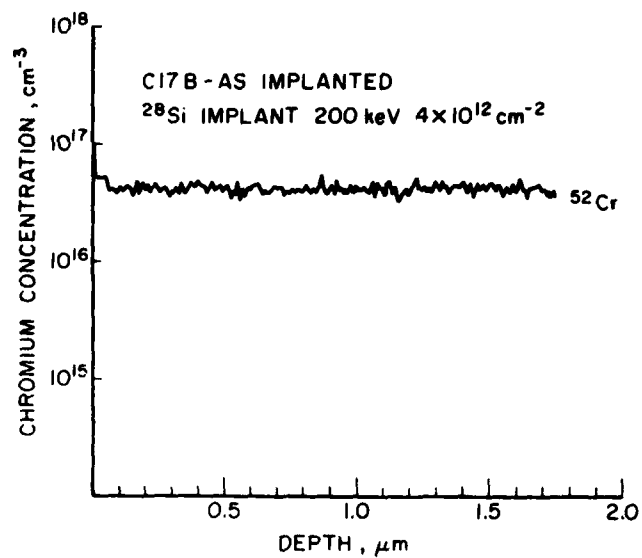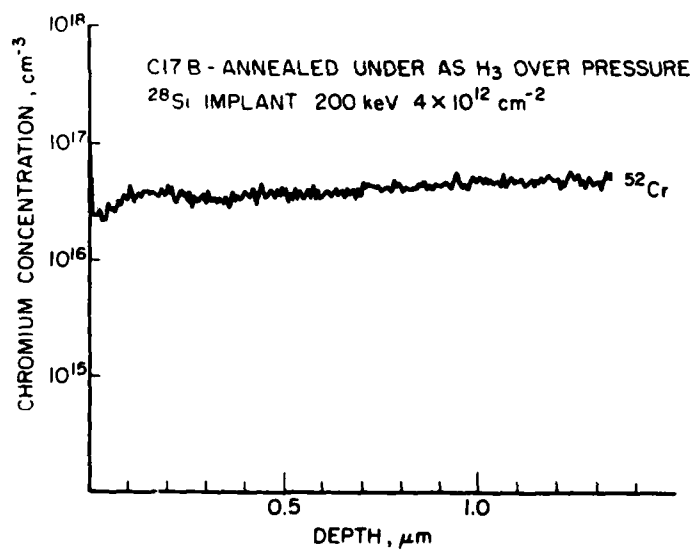
Figure 29. (a) SIMS profile of Cr concentration in low-dose, Si-implanted unannealed GaAs; (b) SIMS profile of Cr concentration in low-dose, Si-implanted capless-annealed GaAs.

under arsenic overpressure. The substrates were Cr-doped with (100) orientation and were grown by Crystal Specialities, Inc., Monrovia, CA. The background Cr concentration was $\sim 5 \times 10^{16}$ cm^{-3}. After capless thermal annealing, a very slight depletion of Cr occurred toward the surface. This low implant dose level is typically used to obtain $\sim 10^{17}$ cm^{-3} carrier concentration for the active layers of microwave FETs.

At a higher implant fluence level (e.g., 3×10^{14} cm^{-2}, 200 keV), the Cr-redistribution effect is enhanced. This is illustrated in Fig. 30 which shows (i) a pronounced Cr depletion below the surface to a depth of ~ 1.5 µm, (ii) an accumulation of Cr at surface, and (iii) a small Cr peak at a depth approximately corresponding to the projected range of the Si implant.
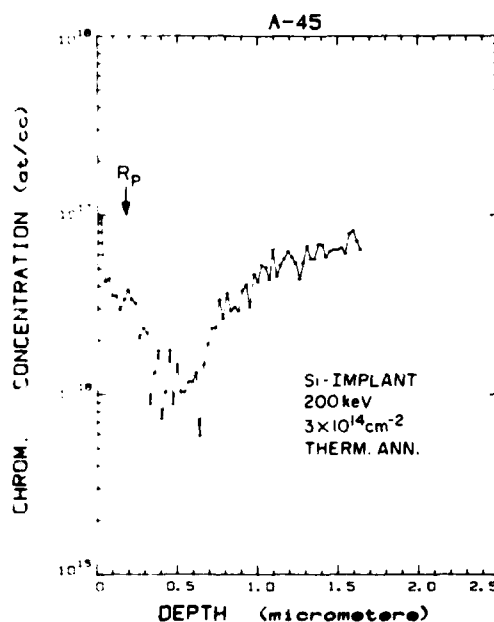
Figure 30. SIMS profile of Cr concentration in Si-implanted (3×10^{14} cm^{-2}, 200 keV) capless-annealed GaAs.

The fluence dependence of Cr redistribution can be observed more closely at higher implant energies because of the increased implant depth associated with high energy implant. Figures 31 and 32 show SIMS profiles of Cr redistribution in two capless-annealed wafers which were implanted at 1 MeV, with fluences of 1×10^{13}, and 3×10^{15} cm^{-2}, respectively. The general behavior of Cr distribution in these wafers is similar to those implanted at 200 keV as have just been described: a broad dose-dependent Cr depletion toward the surface, plus local Cr accumulations in the vicinity of depths $\sim R_p + \Delta R_p$, and at the surface of the wafer.

45

Figure 31. SIMS profiles of ^{52}Cr in low-dose 1-MeV Si-implanted, capless-annealed GaAs.

Figure 32. Cr-concentration profile of high-dose 1-MeV Si-implanted capless-annealed GaAs; Si profile in arbitrary units is also shown.

46

Thus GaAs samples annealed without encapsulant under arsenic overpressure
show either depletion or accumulation of chromium at the surface, depending on
the amount of implant doses: a slight depletion occurred for low-dose implant
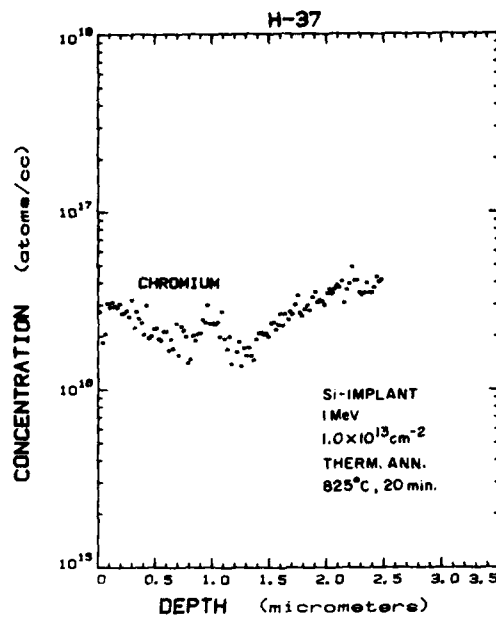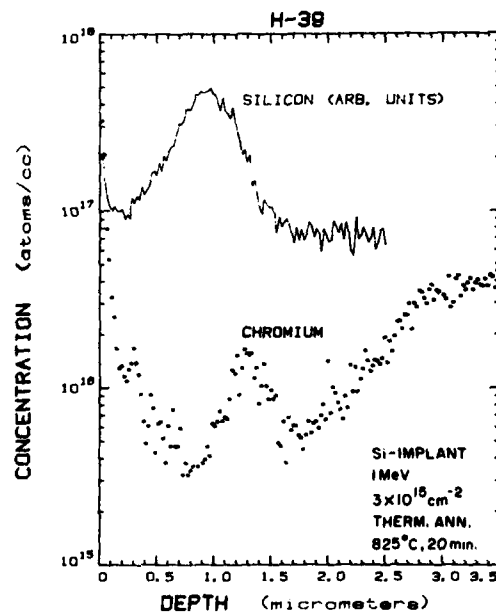and an accumulation (to the mid $\sim 10^{17}$ cm^{-3} Cr concentration) occurred for
high-dose implants. This result is different from samples annealed with
encapsulant on the surface. Figure 33 shows the SIMS profile of a Si$_3$N$_4$
cap-annealed (in N$_2$) sample which was double-implanted with low doses of
3.5×10^{12} cm^{-2} at 200 keV, and 4×10^{11} cm^{-2} at 70 keV. The profile shows a high
($>10^{18}$ cm^{-3}) $\sim$500-Å-deep Cr spike at the surface.
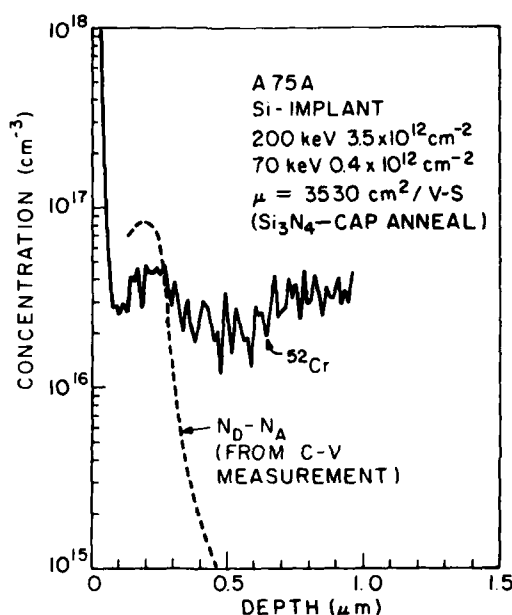
Figure 33. SIMS profile of Cr concentration in low-dose Si-implanted
GaAs thermally annealed with Si$_3$N$_4$ encapsulant. Correspond-
ing electron density profile is also shown.

The Cr redistribution in laser-irradiated high-dose Si-implanted GaAs has
also been investigated. Figure 34 shows a 3×10^{15} cm^{-2}, 200 keV Si-implanted,
1.0 J/cm^2 pulsed ruby-laser-irradiated GaAs; Figure 35 shows a 2.5×10^{15} cm^{-2},
600-keV Si implant irradiated with a 1.5-J/cm^2 pulsed Nd:Glass laser beam.
The pulse width of the laser beam was 25 ns (FWHA). Note that the Cr redis-
tribution in each case consists of a small amount of Cr depletion plus an
accumulation at the surface up to mid $\sim 10^{17}$ cm^{-3}. The Cr depletion is much
less than thermally annealed GaAs implanted with similar dose levels (Fig. 32).

Figure 34. Chromium distribution of Si-implanted $(3\times10^{15}$ cm^{-2}, 200 keV) 1.0 J/cm^2 pulsed ruby-laser irradiated GaAs.
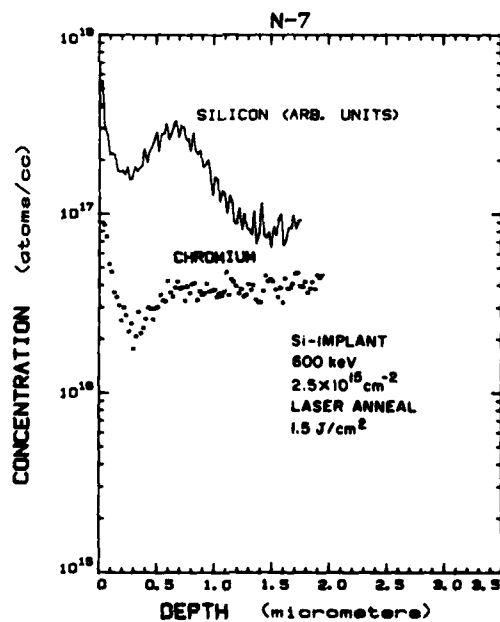
Figure 35. Cr-concentration profile of 600-keV Si-implanted laser-annealed GaAs. Si profile in arbitrary units is also shown.

The measured sheet carrier concentration of 7.4×10^{14} cm^{-2} for the activated n-layer of sample N7 (Fig. 35) after laser irradiation is higher than thermally annealed control samples.

C. CHROMIUM REDISTRIBUTION IN ^{40}Ar-IMPLANTED SI GaAs SUBSTRATES

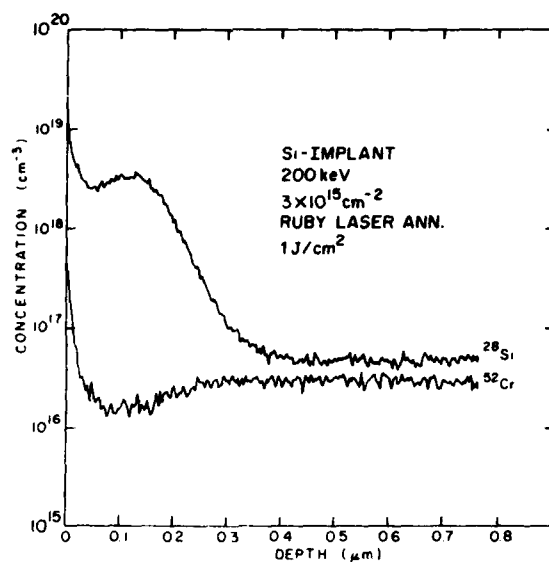We have shown that the measured SIMS profiles on Si-implanted, thermally annealed SI GaAs show strong dependence of ^{52}Cr redistribution on the amount of ^{28}Si dose. To shed more light on this effect, we implanted inert ^{40}Ar ions into SI GaAs at high energies and studied the Cr-redistribution behavior in these samples. Measured SIMS profiles show characteristics similar to those observed in Si-implanted samples; namely, (1) it showed a constant Cr level before the sample was thermally annealed, (2) a "double-valley" depletion of Cr existed in a layer near the surface after the sample was thermally annealed, and (3) the amount of Cr redistribution depended on the implant dose level. SIMS profiles of a 750 keV, 5×10^{13} cm^{-3} Ar-implanted GaAs wafer, before and after thermal anneal, are shown in Fig. 36. An accumulation of chromium, which approximately coincides with the projected range of the implant, exists in the Cr-depletion layer.
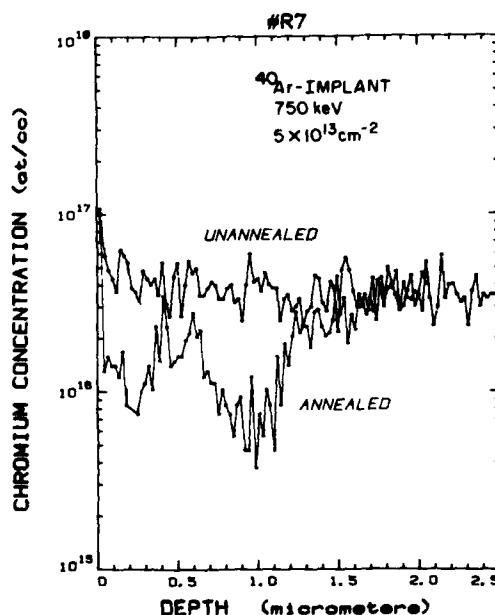
Figure 36. SIMS profile of Cr concentration in ^{40}Ar-implanted GaAs $(5 \times 10^{13}$ cm^{-2}, 750 keV) before and after capless annealing (825°C, 20 min).

At a higher implant fluence the Cr depletion increases and broadens, and the Cr-accumulation peak tends to shift from the position of R_p toward the substrate; also the Cr accumulation is enhanced at the surface. This result is illustrated in Fig. 37, where the Cr profile of a 1×10^{15} cm^{-2} Ar-implanted capless-annealed SI GaAs sample is shown.
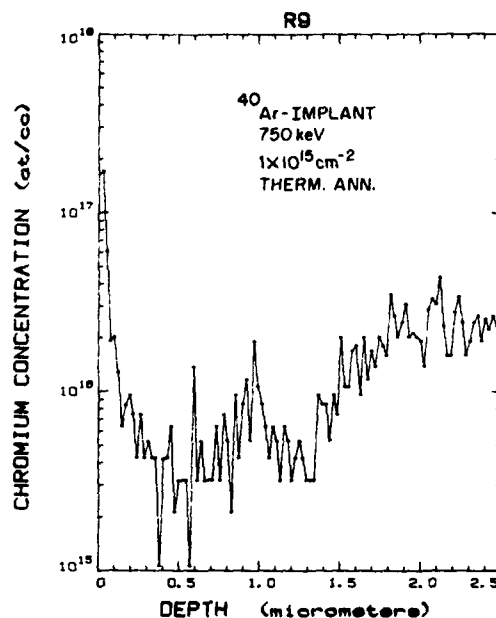
Figure 37. SIMS profile of ^{40}Ar-implanted (1×10^{15} cm^{-2}, 750 keV) capless annealed (825°C, 20 min) GaAs.

D. DISCUSSION

The depletion of chromium in thermally annealed samples is believed to be a result of Cr diffusion [16-18] toward the surface. The very slight amount of depletion in low-dose implanted GaAs (Fig. 29b) is believed due to low implant damage and capless annealing under arsenic overpressure. The presence of a Cr spike in the profile to a depth 200 Å from the surface is likely to be an artifact [16].

The Cr accumulation that extended to a deeper depth (∿1000 Å in Fig. 33) in Si-implanted GaAs annealed with Si_3N_4 encapsulant is similar to what has been reported previously [16,19,20]; it was interpreted [20] as strain-induced

20. A. Lidow, J. F. Gibbons, T. Magee, and J. Peng, "Strain-Induced Gettering by the Thermal Expansion Mismatch Between the Encapsulant and the GaAs Crystals," J. Appl. Phys. 49, 5213 (1978).

gettering caused by thermal expansion mismatch between the encapsulant and the GaAs crystal.

The extended magnitude and depth of Cr depletion in high-dose implanted capless-annealed GaAs (Figs. 30 and 32) is believed to be attributed to enhanced diffusion. The Cr peaks near the surface and at depths close to $\sim R_p + \Delta R_p$ are believed to be a result of damage gettering [21]. Thus, it is speculated that the diffusion (damage enhanced) and the gettering processes during capless annealing are the causes of the Cr-distribution profiles observed. The reduced Cr-redistribution effect in medium-dose implanted GaAs (Fig. 31), and the fact that similar profiles were observed in Ar-implanted capless annealed GaAs (Figs. 36 and 37) further stresses the role of implant damage.

21. C. O. Bozler, J. P. Donnelly, W. T. Lindley and R. A. Reynolds, "Impurity Gettering in Semi-insulating Gallium Arsenide Using Ion-implantation Damage," Appl. Phys. Lett. 29, 698 (1976).

SECTION V

SUMMARY

This report described work performed under the contract during the past year on implantation and annealing studies in GaAs. The implantation of ^{28}Si was carried out at energies between 40 and 1200 keV. High-energy implantation of ^{40}Ar up to 750 keV and its effect on chromium redistribution in GaAs substrates have also been investigated. Significant progress accomplished during this reporting period is summarized below.

- Uniformly doped 1-μm-deep n-layers having mobility of 4450 cm^2/V-s at carrier concentrations of $\sim$2x10^{17} cm^{-3} were produced by multiple implantation and capless thermal annealing.

- Temperature-dependence studies of the capless-annealing process showed considerably higher electrical activation hence lower sheet resistance for high-dose implanted samples annealed at a higher temperature. No significant difference in activation in low-dose ($<$10^{13} cm^{-2}) implanted samples.

- Chromium redistribution studies in thermally annealed Si implants show a strong dependence of Cr redistribution on implant dose. Pulsed-laser-irradiated implants show much less Cr redistribution than thermally annealed GaAs.

- Preliminary studies on ^{40}Ar implanted GaAs showed similar Cr-redistribution effect as in the Si implants. Si implantations in properly Ar-treated samples showed low-dose activation with good mobility.

- Nonalloyed ohmic contacts were formed on laser-irradiated GaAs using Ti-Pt-Au metallization with good surface morphology. Double-frequency laser beam (λ=1.06 and 0.53 μm) was used in the experiment.

- The crystallinity of laser- (or electron beam) irradiated Si-implanted GaAs was studied using reflection high-energy diffraction (RHEED) analysis.

- Preliminary studies on co-implant of ^{28}Si and ^{32}S into GaAs show higher mobility and activation when implants were annealed at a higher temperature.

52

- Activation of 1-MeV implanted GaAs with peak electron density over 1×10^{19} cm^{-3} was demonstrated by using a high-power subbandgap Nd: Glass laser (λ=1.06 μm).

- Finally, the success of producing high quality n-GaAs layers by direct implant of ^{28}Si into SI GaAs was demonstrated, in a concurrent program, by fabrication of high-performance GaAs power FETs operating up to 26 GHz.

REFERENCES

1. S. G. Liu, E. C. Douglas and C. P. Wu, "High-Energy Ion Implantation for Multigigabit-Rate GaAs Integrated Circuit," Annual Report, May 15, 1978 to May 14, 1979, under ONR Contract N00014-78-C-0367.

2. S. G. Liu, E. C. Douglas, C. P. Wu, C. W. Magee, S. Y. Narayan, S. T. Jolly, F. Kolondra, and S. Jain, "Ion Implantation of Sulfur and Silicon in GaAs," RCA Review 41, 227 (1980).

3. S. G. Liu, E. C. Douglas, C. W. Magee, F. Kolondra, and S. Jain, "High-Energy Implantation of Si in GaAs," Appl. Phys. Lett. 37, 79 (1980).

4. M. G. Kendall and A. Stuart, The Advanced Theory of Statistics, (Charles Griffin, London, 1958), Vol. 1, p. 148.

5. W. P. Elderton, Frequency Curves and Correlation, (Cambridge University Press, 1953), 4th ed.

6. L. J. van der Pauw, "A Method of Measuring Specific Resistivity and Hall Effect of Discs of Arbitrary Shape," Philips Res. Rep. 13, 1 (1958).

7. J. R. Arthur, "Vapor Pressures and Phase Equilibria in the GaAs System," J. Phys. Chem. Solids 28, 2257 (1967).

8. S. G. Liu, C. P. Wu and C. W. Magee, "Annealing of Ion-Implanted GaAs with Nd:Glass Laser," AIP Conference Proceedings, No. 50, 603 (1978).

9. S. G. Liu, C. P. Wu and C. W. Magee, "Annealing of Ion-Implanted GaAs with a Pulsed Ruby Laser," Symposium Proceedings on Laser and Electron Beam Processing of Materials, Academic Press, 341 (1980).

10. J. C. Wang, R. F. Wood and P. P. Pronko, "Theoretical Analysis of Thermal and Mass Transport in Ion-Implanted Laser-Annealed Silicon," Appl. Phys. Lett. 33, 445 (1978).

11. P. A. Pianetta, C . A. Stolte and J. L. Hauser, "Pulsed E-Beam and Ruby Laser Annealing of Ion Implanted GaAs," Symposium Proceedings on Laser and Electron Beam Processing of Materials, Academic Press, 328 (1980).

12. P. A. Barnes and A. Y. Cho, "Nonalloyed Ohmic Contacts to n-GaAs by Molecular Beam Epitaxy," Appl. Phys. Lett. 33, 651 (1978).

13. R. L. Mozzi, W. Fabian, and F. J. Piekarcki, "Nonalloyed Ohmic Contacts to N-GaAs by Pulse Electron Beam-Annealed Selenium Implants," Appl. Phys. Lett. 35, 337 (1979).

14. M. N. Yoder, "Ohmic Contacts in GaAs," Solid State Electronics 23, 117 (1980).

15. H. H. Berger, "Models for Contacts to Planar Device," Solid State Electron. $\underline{15}$, 145 (1972). Also, J. Electrochem. Soc. $\underline{119}$, 507 (1972).

16. A. M. Huber, G. Morillot and N. T. Linh, "Chromium Profiles in Semi-insulating GaAs after Annealing with a Si_3N_4 Encapsulant," Appl. Phys. Lett. $\underline{34}$, 858 (1979).

17. R. G. Wilson, P. K. Vasuder, D. M. Jamba, C. A. Evans, Jr. and V. R. Deline, "Chromium Concentrations, Depth Distributions and Diffusion Coefficient in Bulk and Epitaxial GaAs and in Si," Appl. Phys. Lett. $\underline{36}$, 215 (1980).

18. J. Kasahara and N. Watanabe, "Redistribution of Cr in Capless-Annealed GaAs Under Arsenic Pressure," Jap. J. of Appl. Phys. 19, L151 (1980).

19. C. A. Evans, Jr. and V. R. Deline, "Redistribution of Cr During Annealing of [80]Se-implanted GaAs," Appl. Phys. Lett. $\underline{35}$, 291 (1979).

20. A. Lidow, J. F. Gibbons, T. Magee, and J. Peng, "Strain-Induced Gettering by the Thermal Expansion Mismatch Between the Encapsulant and the GaAs Crystals," J. Appl. Phys. $\underline{49}$, 5213 (1978).

21. C. O. Bozler, J. P. Donnelly, W. T. Lindley, and R. A. Reynolds, "Impurity Gettering in Semi-insulating Gallium Arsenide Using Ion-implantation Damage," Appl. Phys. Lett. $\underline{29}$, 698 (1976).

Code 427 Office of Naval Research Arlington, VA 22217	4	Dr. H. C. Nathanson Westinghouse Research and Development Canter Beulah Road Pittsburgh, PA 15235	1

Naval Research Laboratory
4555 Overlook Avenue, S. W.
Washington, D. C. 20375
Code 6811
    6850
	
	1
	1
		Dr. Daniel Chén
		Rockwell International
		  Science Center
		P. O. Box 1085
			1

Defense Documentation Center Building 5, Cameron Station Alexandria, VA 22314	12	Thousand Oaks, CA 91360	
Dr. Y. S. Park AFWAL/DHR Building 450 Wright-Patterson AFB Ohio, 45433	1	Dr. D. Krumn Hughes Research Laboratory 3011 Malibu Canyon Road Malibu, CA 90265 Mr. Lothar Wandinger ECOM/AMSEL/TL/IJ Fort Monmouth, NJ 07003	1 1
ERADCOM DELET-M Fort Monmouth, NJ 07703	1	Dr. Harry Wieder Naval Ocean Systems Center Code 922 271 Catalina Blvd. San Diego, CA 92152	1
Texas Instruments Central Research Lab M.S. 134 P. O. Box 225936 Dallas, TX 75265 Attn: Dr. W. Wisseman	1	Dr. William Lindley MIT Lincoln Laboratory F124 A, P. O. Box 73 Lexington, MA 02173	1
Dr. R. M. Malbon/M.S. 1C Avantek, Inc. 3175 Bowers Avenue Santa Clara, CA 94303	1	Commander U.S. Army Electronics Command V. Gelnovatch (DRSEL-TL-IC)	1
Mr. R. Bierig Raytheon Company 28 Seyon Street Waltham, MA 02154	1	Fort Monmouth, NJ 07703 RCA Microwave Technology Center	 1
Dr. R. Bell, K-101 Varian Associates, Inc. 611 Hansen Way Palo Alto, CA 94304	1	Dr. F. Sterzer Princeton, NJ 08540	

Hewlett-Packard Corporation   1
Dr. Robert Archer
1501 Page Mill Road
Palo Alto, CA   94306

Watkins-Johnson Company   1
E. J. Crescenzi, Jr./
  K. Niclas
3333 Hillview Avenue
Stanford Industrial Park
Palo Alto, CA   94304

Commandant   1
Marine Corps
Scientific Advisor (Code AX)
Washington, D. C.   20380

Communication Transistor Corp.   1
Dr. W. Weisenberger
301 Industrial Way
San Carlos, CA   94070

Microwave Associates   1
Northwest Industrial Park
Drs. F. A. Brand/J. Saloom
Burlington, MA   01803

Commander, AFAL   1
AFWAL/AADM
Dr. Don Rees
Wright-Patterson AFB, Ohio   45433

Professor Walter Ku   1
Phillips Hall
Cornell University
Ithaca, NY   14853

Commander   1
Harry Diamond Laboratories
Mr. Horst W. A. Gerlach
2800 Powder Mill Road
Adelphia, MD   20783

Advisory Group on Electron   1
  Devices
201 Varick Street, 9th floor
New York, NY   10014

D. Claxton   1
MS/1414
TRW Systems
One Space Park
Redondo Beach, CA   90278

Professor L. Eastman   1
Phillips Hall
Cornell University
Ithaca, NY   14853

AIL TECH   1
612 N. Mary Avenue
Sunnyvale, CA   94086
Attn: G. D. Vendelin

Professors Hauser and   1
  Littlejohn
Department of Electrical Engr.
North Carolina State University
Raleigh, NC   27607

Professor J. Beyer   1
University of Wisconsin-Madison
750 University Avenue
Madison , Wisconsin   53706

General Electric Company   1
Attn: W. Perkins
Electronics Lab 3-115/B4
P. O. Box 4840
Syracuse, NY   13221

Professor Rosenbaum and Wolfe   1
Washington University
Semiconductor Research Laboratory
P. O. Box 1127
St. Louis, Missouri   63130

T. J. Magee   1
ARACOR
1223 Arques Avenue
Sunnyvale, CA   94086

TIC